

# Dark Matter in the Local Universe

Gustavo Yepes

*Departamento de Física Teórica M-8, Universidad Autónoma de Madrid, Cantoblanco 28049 Madrid Spain*

Stefan Gottlöber

*Leibniz Institut für Astrophysik, An der Sternwarte 16, 14482 Potsdam, Germany*

Yehuda Hoffman

*Racah Institute of Physics, The Hebrew University of Jerusalem, 91904 Givat Ram, Israel*

---

## Abstract

We review how dark matter is distributed in our local neighbourhood from an observational and theoretical perspective. We will start by describing first the dark matter halo of our own galaxy and in the Local Group. Then we proceed to describe the dark matter distribution in the more extended area known as the Local Universe. Depending on the nature of dark matter, numerical simulations predict different abundances of substructures in Local Group galaxies, in the number of void regions and the abundance of low rotational velocity galaxies in the Local Universe. By comparing these predictions with the most recent observations, strong constraints on the physical properties of the dark matter particles can be derived. We devote particular attention to the results from the Constrained Local Universe Simulations (CLUES) project, a special set of simulations whose initial conditions are constrained by observational data from the Local Universe. The resulting simulations are designed to reproduce the observed structures in the nearby universe. The CLUES provides a numerical laboratory for simulating the Local Group of galaxies and exploring the physics of galaxy formation in an environment designed to follow the observed Local Universe. It has come of age as the numerical analogue of Near-Field Cosmology.

### *Keywords:*

98.35.Gi, 98.52.Wz 98.56.-p 98.65.Dx 95.35.+d 98.90+s

---

## 1. Introduction

It is widely attributed to Fritz Zwicky (1933) the introduction of the name *dark matter* (DM) to account for the non-visible mass required to explain the large velocity dispersion of the galaxies in the Coma cluster that he derived by applying the Virial Theorem. But, in fact, he was referring to the term used first by the Dutch astronomer Jaan Oort (1932) one year earlier. Oort studied the dynamics of the brightest stars in the disk of the Milky Way (MW). From his analysis he deduced that the total density exceeds the density of visible stellar populations by a factor of up to 2. This limit is often called the Oort limit. Thus, he concluded that the amount of invisible matter in the Solar vicinity could be approximately equal to the amount of visible matter. He named it, for the first time, this invisible component as *dark matter*. Later on, Babcock (1939) measured, for the first time, the mass distribution in the Andromeda Galaxy (M31) from the radial velocity curves derived from optical emission line regions. He concluded that the mass profile of M31 monotonically increases from the centre outwards, up to 20 kpc, the maximum distance he could observe. In the late 50's, the first 21-cm observations (van de Hulst et al., 1957), corroborated the earlier optical results from Babcock and clearly indicated that the rotation curve of M31 flattens off at around 35 kpc with no indication of a decay. During the late 70's (Bosma, 1978) and early 80's, (Rubin et al., 1980), more observations of M31 and other spiral galaxies clearly indicated that their rotation curves were flat out

to large distances from the optical emission (see e.g. Einasto, 2009) for a more detailed description of the historical development of the DM concept).

A completely different, more theoretically based, approach in the determination of the total masses of MW and M31 was used by Kahn and Woltjer (1959). The evidence that M31 has a negative redshift of about  $120 \text{ km s}^{-1}$  towards our Galaxy can be explained, if both galaxies, M31 and MW, form a gravitationally bound system. A negative radial velocity indicates that these galaxies have already passed the apocenter of their relative orbit and are presently approaching each other. From the approaching velocity, the mutual distance, and the time since passing the pericenter (taken as the present age of the Universe) the authors calculated the total mass, assuming a two body point-like system. They found that the combined mass of M31 and MW is  $M_{tot} \geq 1.8 \times 10^{12} M_{\odot}$ . This value is a factor of  $\sim 10$  higher than the conventional mass estimates of the two galaxies ( $\sim 2 \times 10^{11} M_{\odot}$ ). This method is known as the *Timing Argument* and it is one of the first observational evidence that the total gravitating mass of the Local Group (LG) exceeded the visual one by almost an order of magnitude. Nevertheless, the hypotheses in which the Timing Argument is based have not been tested until recently, when simulations can make possible to trace back the formation history of LG-like objects. We will come back to this in §5.1.

There is now an overwhelming amount of observational evidence, at many different scales, that firmly supports the idea that there exists much more matter in the Universe than just the luminous matter. The ratio between the dark and the visible matter components grows with scale. It is widely assumed that gravitational instability of the primordial density perturbations in the collisionless DM fluid is the main mechanism that drives the formation of structure. The standard  $\Lambda$  Cold Dark Matter ( $\Lambda$ CDM)-model, where  $\Lambda$  is the Cosmological Constant, of cosmological structure formation describes very well the observations of the large scale structure (LSS), (see e.g. Frenk and White, 2012, for a review).

At present, the parameters of the model have been determined with very high precision (Planck Collaboration et al., 2013). Despite all the success of the model to explain LSS, the formation of small scale structure seems to be an open problem. It has been known for a long time that the model predicts more small scale structures than observed (Klypin et al., 1999; Moore et al., 1999; Diemand et al., 2007; Springel et al., 2008).

Numerical N-body simulations have given us a clear picture of how DM is structured at different scales. At large scales, DM is distributed in the universe in the form of a web, the so called *cosmic web* (Bond et al., 1996). Observationally, the distribution of galaxies in the universe, as well as the distribution of total matter, as inferred from its gravitational lensing and reconstructions from large galaxy surveys give also the appearance that mass and light are distributed in a web-like structure dominated by linear filaments and concentrated compact knots, thereby leaving behind vast extended regions of no or a few galaxies and of low density (Jasche et al., 2010; Muñoz-Cuartas et al., 2011; Wang et al., 2012; Kitaura et al., 2012). Direct mapping of the mass distribution by weak lensing reveals a time evolving loose network of filaments, which connects rich clusters of galaxies (Massey et al., 2007). The extreme low resolution of the weak lensing maps cannot reveal the full intricacy of the cosmic web, and in particular the difference between filaments and sheets, yet they reveal a web structure that serves as a gravitational scaffold into which gas can accumulate, and stars can be built.

Our Local Universe is the best place to test the predictions of the  $\Lambda$ CDM model down to the smallest scales given by the free streaming of the DM particles. Therefore, the Local Universe can be considered to be a cosmic laboratory to attempt to identify the nature of DM. In the past years there has been an enormous experimental effort devoted to identify the particle physics candidate for DM (see e.g. Strigari, 2013, for a recent review). Underground direct detection experiments try to find the signature of the elusive dark matter particles of the galactic halo when they weakly interact with the nuclei of detector's material (noble gas, crystalline salt, semiconductors, etc). On the other hand, the FERMI satellite is now searching for the gamma photons coming from disintegration or annihilation of the dark matter particles, at the Milky Way centre, in its dwarf galaxy satellites, or even in extragalactic sources like the nearby Andromeda Galaxy or in Virgo, the closest galaxy cluster to us. The basic hypothesis behind all these experimental efforts is that the constituent of dark matter is a non-baryonic Weakly Interacting Massive Particle (WIMP) like the neutralino, that is predicted in Supersymmetry theories.

On the other hand, there are other probes that try to measure the level of structures formed by gravita-

tional growth of DM fluctuations at small scales, where the predictions for abundance of low mass objects strongly depend on the individual mass of the DM particles. In this regard, the number of satellite galaxies around our Milky Way, or the number of low mass HI galaxies in our local neighbourhood are two excellent observational tests for dark matter models. But, a direct comparison between observations and theoretical predictions must be done with caution. The dynamics of our Local Universe has some special features due to the peculiar distribution of the matter around us. Any realistic simulation of structure formation in a particular dark matter model should account for these features before a reliable comparison with observations can be made. Otherwise, the comparison could be biased due to the cosmic variance.

There have been some attempts to minimize the effect of cosmic variance by simulating the formation of cosmological structures which are designed to resemble our own Local Universe. The so-called CLUES (Constrained Local UniversE Simulation, <http://clues-project.org>) collaboration is trying to do so by imposing observational constraints on the otherwise random realizations of a cosmological initial density perturbation field. As a result, the structures formed reproduces the main features of the observed most massive clusters and superclusters such as Coma, Virgo or the Local Supercluster. Thus, LG-like objects are formed in an environment that resembles the real one. In this context, the CLUES Local Groups can be considered as numerical proxies that can serve to study issues such as:

- how typical our LG is and what can be learnt from it about structure formation at large;
- the structure of the stellar halos in the LG;
- tidal streams and the formation history of the LG;
- the missing satellites problem;
- how does the baryon physics affect the Dark Matter distribution;
- the nature of nearby dwarf galaxy associations beyond the LG;
- improved predictions for Dark Matter detection;
- galaxy formation and environmental dependence in the framework of the cosmic web;

In the upcoming era of the GAIA<sup>1</sup> and PANDAS<sup>2</sup> observations of the LG, simulations like those performed within the framework of CLUES are the numerical counterparts. The combined high quality observations and detailed simulations will shed new light on the formation history of the LG and will provide a new framework for understanding its cosmological implications.

In this review we try to summarize the main results achieved within the CLUES collaboration during the past years on several of the above mentioned items. The “L” in the CLUES stands for “Local” yet local is not a well defined concept. Throughout the paper we use the term “Local” to denote a finite region of the universe which harbours the LG close to its center and that extends over linear scales ranging typically from a very few to a few tens of Megaparsecs.

The paper is structured as follows: In §2 we give a brief description of the CLUES project and summarize the numerical experiments that have been done so far. Then in §3 we focus on the study of the dark matter distribution in the Local Group and how baryon physics affects the distribution of dark matter, which is of extreme importance for experiments of dark matter detection. In §4 we review the main results from CLUES simulations on the formation histories of the Local Group and how unique the LG is as compared with other binary systems formed in dark matter N-body simulations. We continue in §5 with a discussion of the estimation of the total mass of LG based on different mass estimators, including the timing argument, and how well these work on simulations. We move to larger scales and describe in §6 how the cosmic web of dark matter in the Local Universe can be used for Near-Field Cosmological studies. In §7 we show how the Local Universe can also be used as a cosmic laboratory to discern among different candidates to dark matter. We conclude in §8 with a summary of the main results presented in this review.

---

<sup>1</sup><http://www.gaia.esa.int>

<sup>2</sup><https://www.astrosci.ca/users/alan/PANDAS/>

## 2. Simulating the Local Universe: The CLUES project

The Local Universe is the best observed part of the universe in which least massive and faintest objects can be detected and studied in detail. These observations resulted in a new research field called *Near-Field Cosmology* and have motivated cosmologists to study the LG archaeology in their quest for understanding galaxy formation and the play dark matter has on it. This also motivated the CLUES collaboration to perform a series of numerical simulations of the evolution of the local universe. For these simulations we constructed the initial conditions based on the observed positions and peculiar velocities of galaxies in the Local Universe. These simulations reproduce the local cosmic web and its key players, such as the Local Supercluster, the Virgo cluster, the Coma cluster, the Great Attractor and the Perseus-Pisces supercluster. Such constrained simulations cannot directly constrain small scale structure on sub-megaparsec scales, yet they enable the simulation of objects on these scales within the correct environment. Therefore, such simulations provide a very attractive possibility of simulating the Local Group of galaxies within the right environment. We have used these constrained simulations as a numerical Near-Field Cosmological Laboratory for experimenting with the complex gravitational and gasdynamical processes that leads to the formation and evolution of galaxies like our own MW and its neighbour, M31.

### 2.1. Observational Data

Observational data of the nearby universe is used as constraints on the initial conditions and thereby the resulting simulations reproduce the observed large scale structure. The implementation of the Hoffman and Ribak (1991) algorithm of constraining Gaussian random fields to follow observational data and a description of the construction of constrained simulations can be found in detail in Kravtsov et al. (2002) and in Klypin et al. (2003). Here, we briefly describe the observational data used so far.

To set up the CLUES initial conditions we used radial velocities of galaxies drawn from the MARK III (Willick et al., 1997), SBF (Tonry et al., 2001) and the Karachentsev et al. (2004) catalogues. Peculiar velocities are less affected by non-linear effects and are used as constraints as if they were linear quantities (Zaroubi et al., 1999). The other constraints are obtained from the catalogue of nearby X-ray selected clusters of galaxies (Reiprich and Böhringer, 2002). The data constrain the simulations on scales larger than  $\approx 5h^{-1}\text{Mpc}$  (Klypin et al., 2003). It follows that the main features that characterize the Local Universe (e.g. Virgo, Local Supercluster, Coma, Great Attractor, etc) are all reproduced by the simulations. The small scale structure is hardly affected by the constraints and is essentially random.

Currently, the Cosmic Flow 2 survey with more than 8300 galaxies which extends to 12,000 km/s with a median error on distances of  $\sim 15\%$  (Courtois and Tully, 2012a,b; Tully and Courtois, 2012; Tully et al., 2013) is used to set up initial conditions for the next generation CLUES simulations.

### 2.2. Constrained Initial conditions

The Hoffman-Ribak algorithm is used to generate the initial conditions as constrained realizations of Gaussian random fields on a  $256^3$  uniform mesh, from the observational data mentioned above. Since these data only constrain scales larger than a very few Mpc, we have performed a series of different realizations in order to obtain one which contains a LG candidate with the correct properties (e.g. two halos with proper position relative to each-other, mass, negative radial velocity, etc). High resolution extension of the low resolution constrained realizations were then obtained by creating an unconstrained realization at the desired resolution, FFT-transforming it to  $k$ -space and substituting the unconstrained low  $k$  modes with the constrained ones. The resulting realization is made of unconstrained high  $k$  modes and constrained low  $k$  ones.

The constrained simulations performed so far do not account for the shift of the objects with respect to the unperturbed background. Using the Reverse Zeldovich Approximation for constructing the initial conditions improves the quality substantially (Doumler et al., 2013a,b,c) and it is being used in the next generation CLUES simulations.

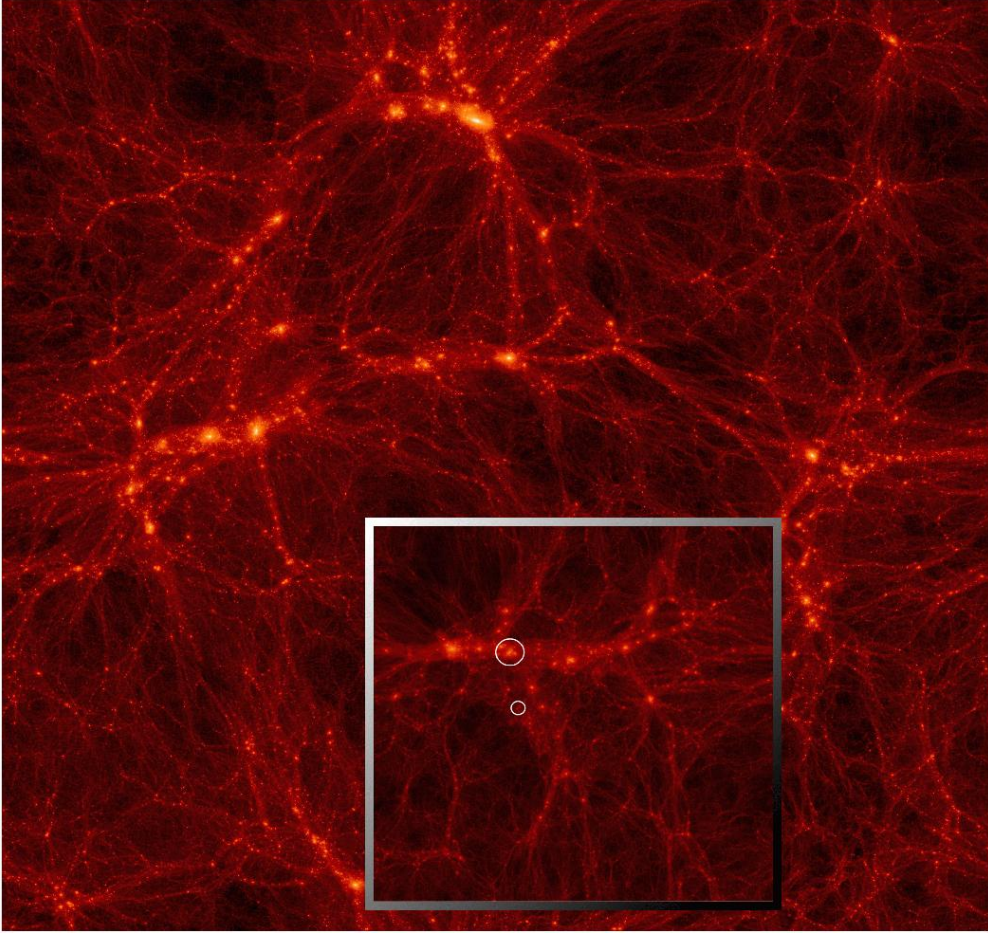


Figure 1: Dark matter density in two constrained simulations in a box of  $160 h^{-1}\text{Mpc}$  size and  $64 h^{-1}\text{Mpc}$  size (smaller inset) with different underlying random realizations

### 2.3. Constrained Simulations of the full box

Using the above initial conditions, we carried out the simulations using the publicly available N-body + SPH code GADGET2 (Springel, 2005).

Two different computational volumes have been used. To study the structures in the Local Universe, a box of  $160 h^{-1}\text{Mpc}$  was simulated. This box is nevertheless, too big to be able to study in detail the internal structure of LG-like objects. Therefore, for the study of the LG and the Local Volume (few Mpc around the LG) a smaller computational box of  $64 h^{-1}\text{Mpc}$  was used.

In Fig. 1 we compare the DM distribution of the constrained simulations in the two computational volumes. As mentioned above, the small scale structure is added in these simulations by random modes according to the underlying cosmological model. The large plot corresponds to the DM distribution in the  $160 h^{-1}\text{Mpc}$  volume and the inset plot shows the DM in the smaller box of  $64 h^{-1}\text{Mpc}$ . The two simulations use the same observational constraints but completely different random phases for the remaining small scale perturbations. Nevertheless it is impressive how well the large scale structure - the Local Super-cluster - is reproduced in both simulations (see Table A.3 for further details).

To find the LG we first identify the Virgo cluster (the large circle in Fig. 1). Then we search for an object which closely resembles the LG and is in the right direction and distance to Virgo (the small circle in Fig. 1). Since the small scale structure is unconstrained, the only possibility to obtain a LG-like object is

to produce many different realizations with the same constrains. Such procedure has yielded 3 good LG-like objects out of 200 constrained initial conditions.

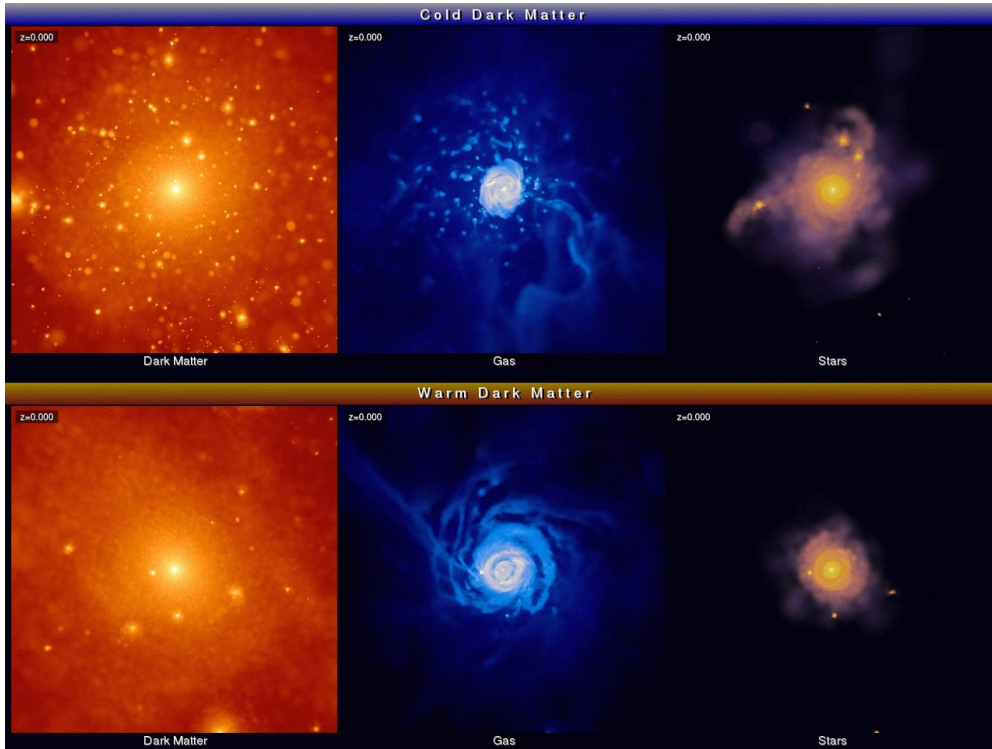


Figure 2: Comparison of a CDM and WDM simulations of a galaxy in the Local Group (Top: CDM, Bottom: WDM; from left to right DM, gas, stars)

#### 2.4. Zoomed Simulations of the Local Group

In order to study the evolution of the LG in more detail we performed zoomed simulations of the evolution of the Local Volume. To this end we have identified spherical regions around the LG candidate at redshift  $z = 0$  and used initial conditions with higher resolution in this region. They were constructed following the prescription set out in Klypin et al. (2001). The main idea is to keep high resolution in the sphere of interest and to decrease the resolution in shells with increasing radius up to a low resolution ( $256^3$  particles) in the rest of the box. By construction we keep the same phases so that the high and low resolution simulations can be directly compared.

In some of the CLUES simulation we replace, in the high resolution area, the Dark Matter particles by pairs of DM and gas particles and follow their evolution using the entropy-conserving SPH version of the GADGET2 code (Springel and Hernquist, 2002) in order to reduce numerical overcooling. Assuming an optically thin primordial mix of hydrogen and helium the radiative cooling is computed following Katz et al. (1996) and photoionization by an external uniform UV background is computed following Haardt and Madau (1996). Finally, star formation is produced from a two-phase interstellar medium of hot and cold gas clouds using a subgrid model (Yepes et al., 1997; Springel and Hernquist, 2003). Including gas-dynamical processes in the simulation one can show that also the DM distribution is changed as well.

As an example of what the CLUES gasdynamical simulations look like, we compare in the upper and lower part of Fig. 2 a Cold and a Warm Dark Matter (CDM and WDM, respectively) simulation of a galaxy in the LG object. On the left panel of this figure, the DM distribution is shown. The middle panel shows the gas and the stars are in the right one. The gaseous and the stellar disks can be clearly seen.

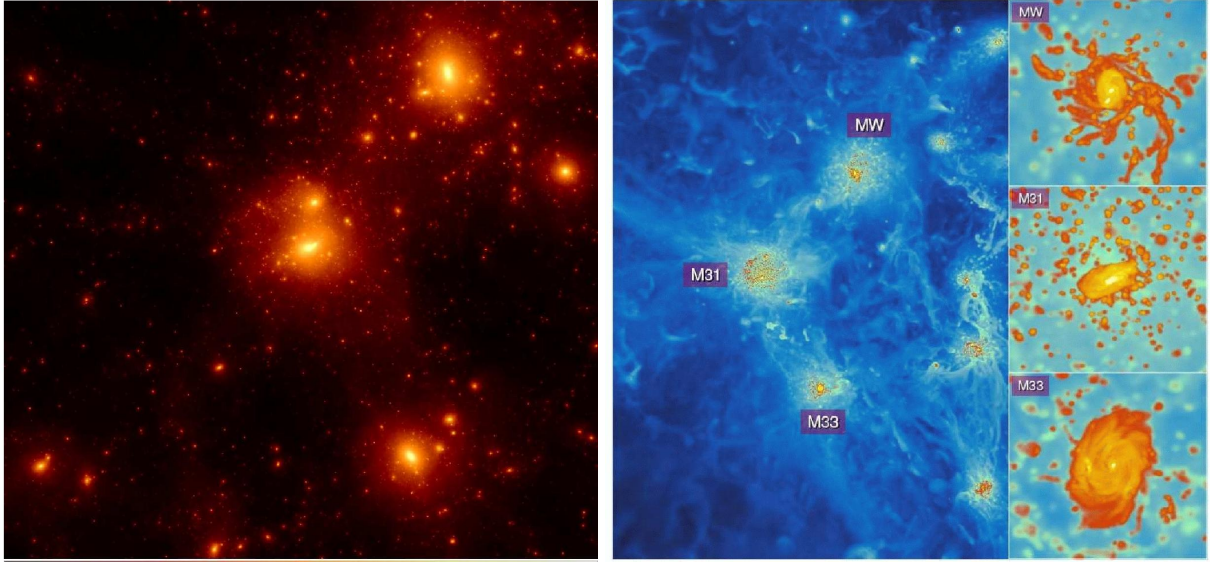


Figure 3: The dark matter distribution of the Local Group candidate found in the dark matter only LG64-3 CLUES simulation (Left) and the gas distribution in the same object from the LG64-3 gasdynamical SPH simulation. The area is approximately  $2 h^{-1}\text{Mpc}$  across.

In Tables A.3 and A.4 of the Appendix we summarize the main features of the CLUES simulations done so far.

### 3. Dark Matter in the Local Group

The observational evidence that the rotation curves of M31 and other spirals are flat suggest that the radial distribution of total matter (stars, gas and dark matter) follow a near isothermal profile with  $\rho(r) \propto r^{-2}$ . Since dark matter is the dominant component, it should also follow such kind of profile. In the early 90s the N-body simulations showed that CDM halos do follow a rather universal density profile parametrized by the so-called NFW formula (Navarro et al., 1997).

$$\rho_{NFW}(r) = \frac{4\rho_s}{\frac{r}{r_s}\left(1 + \frac{r}{r_s}\right)^2} \quad (1)$$

where  $\rho_s$  and  $r_s$  are characteristic density and radius. This fit presents a singularity at  $r \rightarrow 0$ , although the total integrated mass is finite. This sharp rise of the density at the halo centre forms a “cusp”. The NFW has been generalized to allow for different values of the asymptotic slopes towards the centre and to the outskirts.

$$\rho(r) = \frac{2^{(c-\alpha)/\beta} \rho_s}{\left(\frac{r}{r_s}\right)^\alpha \left(1 + \left(\frac{r}{r_s}\right)^\beta\right)^{(c-\alpha)/\beta}} \quad (2)$$

giving the possibility to fit profiles that are cuspier ( $\alpha > 1$ ) or cored ( $\alpha < 1$ ). The core-cusp problem has been a subject of many recent studies, based both on observational data as well as on results from very high-resolution N-body simulations (see eg. de Blok (2010) for a review). The latest numerical results have favored another kind of fitting formula for the density profile of dark matter halos (Navarro et al., 2010; Di Cintio et al., 2013)

$$\rho_E(r) = \frac{\rho_{-2}}{e^{2n \left[ \left(\frac{r}{r_{-2}}\right)^{\frac{1}{n}} - 1 \right]}} \quad (3)$$

where  $r_{-2}$  is the radius where the logarithmic slope of the density profile equals -2 and  $n$  is a parameter that describes the shape of the density profile. The  $r_{-2}$  scale radius is equivalent to  $r_s$  of the NFW profile, and the density  $\rho_{-2} = \rho(r_{-2})$  is related to the NFW one through  $\rho_{-2} = \rho_s/4$ . This profile gives also a finite total mass, but its logarithmic slope decreases inwards more gradually than a NFW, with no asymptotic slope at the centre. This profile is known as the Einasto profile, since it was first proposed by Jaan Einasto in 1965 to model the kinematic of stellar systems.

Knowledge on the DM distribution in the Local Group, and beyond, is essential to any DM detection experiment. This is certainly valid for the indirect detection channel of gamma rays from annihilation/disintegration of DM particles. Knowledge of the full phase space distribution of the DM particles in the Solar neighbourhood is critical for the proper interpretation of direct detection terrestrial experiments. However, this knowledge of the DM distribution is astronomically severely hindered. Despite the fact that the MW galaxy is the best studied of all galaxies, our position inside one of its spiral arms makes it difficult to study accurately the total mass distribution, compared with external galaxies. This situation can be remedied by the use of numerical simulations and experiments.

There are different methods to derive the total gravitating mass of our Galaxy, depending on the distance from us (see eg. Strigari (2013)). Within the central few parsecs, the contribution of dark matter and the disk stars is not very important. The mass is dominated by the bulge and the central black hole, which is estimated to have a mass of  $4 \times 10^6 M_\odot$ . Assuming that the dark matter follows a NFW profile, the integrated mass of dark matter is no more than a few 1000  $M_\odot$  within the few kpc around the centre. Thus, it is not possible, with the current observations, to derive the asymptotic slope of the dark matter mass profiles. It is expected, from results of numerical simulations, that the density profile may be steeper and cuspier than the one given by NFW fit due to the adiabatic compression of the DM in response to the collapse of baryons to the centre (Gnedin et al., 2011).

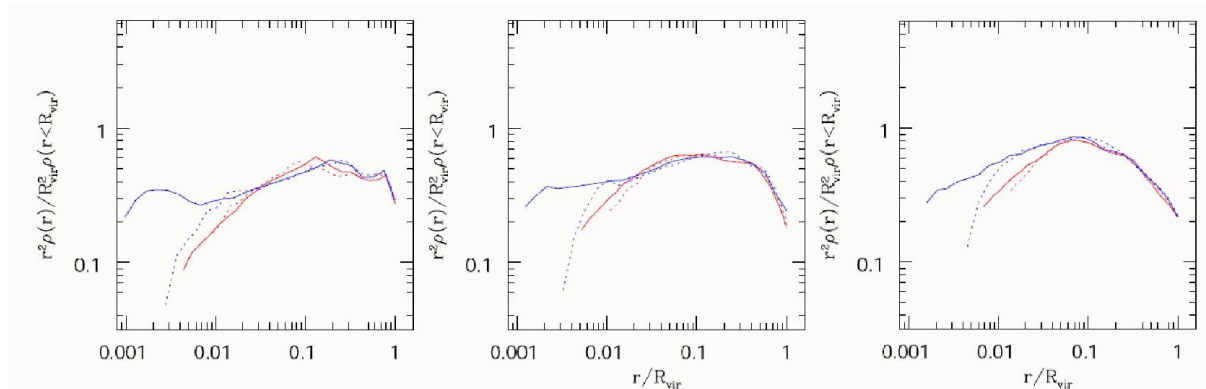


Figure 4: The DM density profiles, scaled by  $r^2$ , for the three main halos of the LG found in the LG64-3 CLUES simulation (see Table A.4). From left to right: M31, MW and M33, named according to the descending masses. The results from the dark matter only simulation are shown in solid red while the same objects simulated with baryons (gas and stars) are shown in solid blue. The dotted lines represent the results from simulations with 8 times less resolution in mass. (Figure taken from Luis A. Martinez-Vaquero’s PhD thesis)

Fig. 4 shows the DM density profile of the three most massive galaxies (MW, M31 and M33, hereafter) of the LG64-3-DM and LG64-3-SPH high-resolution CLUES simulations (see Table A.4). As can be seen, there are substantial differences in the slopes of the dark matter when baryons and their physical effects (cooling, star formation, etc) are taken into account. While in the collisionless DM only simulations the profiles are well in agreement with NFW, the DM profiles in the gasdynamical run have steeper slopes, closer to -2 at the inner parts. This effect on the DM caused by the cooled baryons that sink to the centre of the DM halos is known as “adiabatic contraction” and it can be modelled analytically (Gnedin et al., 2011, and references therein), giving a reasonable good approximation to the simulation results. The inclusion of this effect is crucial for a correct estimation of the DM density at the galactic centre and can make substantial differences in the estimation of the gamma ray fluxes coming from dark matter annihilation (Gomez-Vargas



et al., 2013).

Another effect that can be observed when physical processes involving baryons are considered in the simulations is that the shape of the DM halo is different from that obtained in simulations containing only DM. We have also quantitatively studied this effect by calculating the eigenvalues and eigenvectors of the tensor of inertia at different distances from the Galactic Centre in the CLUES galaxies. Fig. 5 shows that the

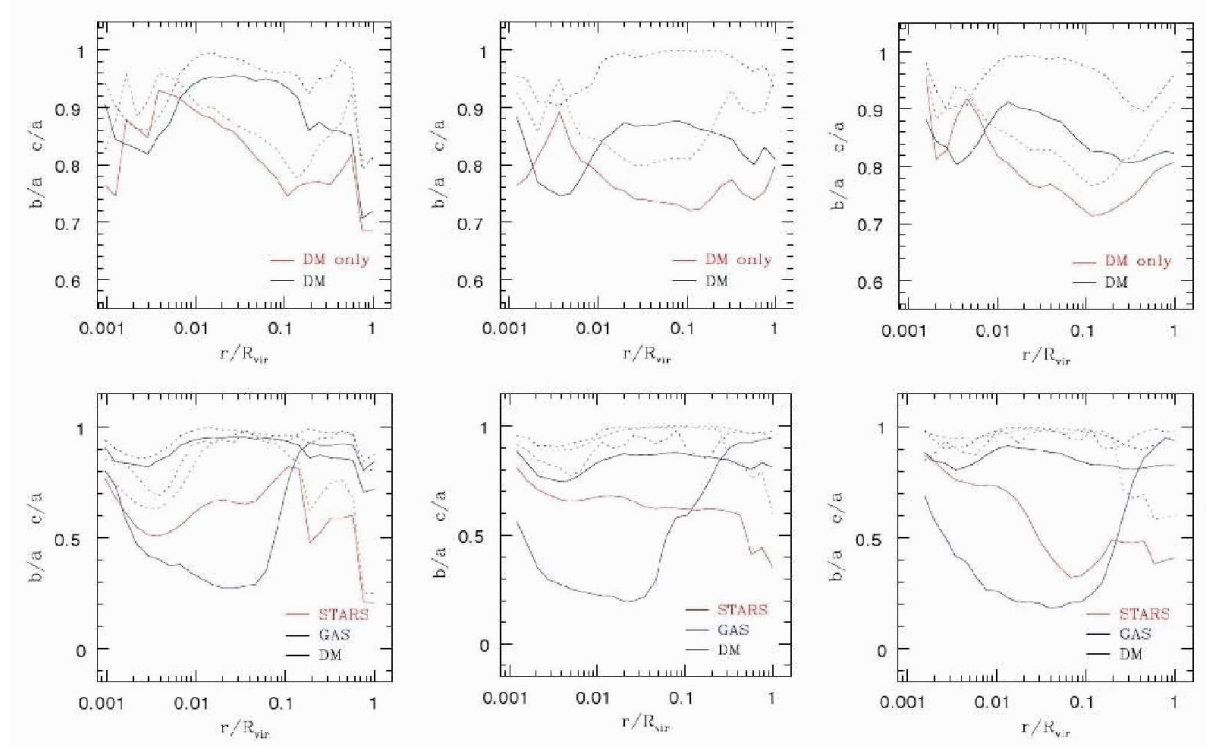


Figure 5: Ratios of the 3 eigenvalues ( $a > b > c$ ) of the inertia tensor (solid curves represent  $c/a$ , and dotted represent  $b/a$ ), corresponding to the distribution of stars, gas and DM for the three main halos of the LG found in the LG64-3 CLUES simulation. From left to right: M31, MW and M33, named according to the descending masses. The results from the DM-only simulation is shown in the upper row, while the results for the gasdynamical simulation is shown in the lower row. (Figure taken from Luis A. Martinez-Vaquero’s PhD thesis)

ratio of the eigenvalues of the inertia tensor ( $a > b > c$ ) approaches 1, indicating that the DM distribution in MW type halos becomes more spherical when baryons are taken into account. These results gives theoretical support to the common assumption of spherical symmetry used in models that try to reconstruct the mass distribution of the MW from a variety of observations (e.g. Catena and Ullio, 2010). From observations, the situation is far from being settled down. Depending on the kind of mass tracer used (eg. stars, HI or stellar streams) the shape of the MW DM halo ranges from spherical, prolate, oblate or triaxial. This issue is expected to be resolved by upcoming larger scale surveys of the phase space distribution of stars in the MW, like GAIA, from which the gravitational potential can be recovered, and thereby also the distribution of DM.

### 3.1. The LG as a Dark Matter Laboratory: WDM vs CDM

As we have mentioned above, our Galaxy is the only place we can measure dark matter structures at the shortest scales. Therefore, we can use the observational information on the satellite population of MW and M31 to compare with the predictions of simulations of MW-type halo formation in different dark matter scenarios. We have also mentioned the problem the standard  $\Lambda$ CDM model has to explain the number of satellite galaxies in the LG. High resolution N-body simulations predict an order of magnitude more

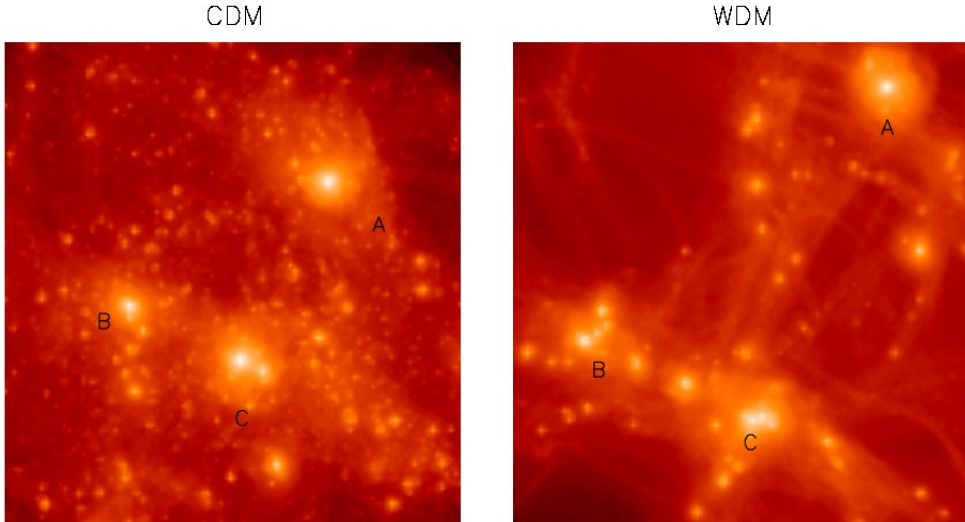


Figure 6: A comparison of the dark matter distribution of the Local Group object in two different dark matter scenarios, the standard CDM (CLUES simulation LG64-3) and in a WDM scenario, assuming that the dark matter particles have a mass of 1 keV, (CLUES simulation LG64-3-WDM) (Figure taken from Libeskind et al. (2013a))

subhalos capable of hosting visible satellites than are detected in the LG. The usual explanation to this discrepancy within the  $\Lambda$ CDM model is to resort to the existence of biases between the satellite galaxies and dark matter sub halos hosting them. The baryonic feedback processes can efficiently suppress galaxy formation inside them. Nevertheless, there is not only an inconsistency in the number of galaxy satellites with respect to halos, but also about the kinematics of the observed dwarf spheroidals (dSphs) in the MW. The velocity profiles of the most massive subhaloes found in high-resolution simulations of a typical  $10^{12} M_{\odot}$  dark matter halo (Boylan-Kolchin et al., 2011) show a large peak circular velocity (assuming that dark matter follows an NFW profile). They are too dense to host any of the bright ( $L_V > 10^5 L_{\odot}$ ) MW satellites. Moreover, they should produce larger annihilation fluxes than the current detection limits on dwarf galaxies set by the FERMI satellite. Possible solutions to this puzzle have been explored within the  $\Lambda$ CDM model by Boylan-Kolchin et al. (2012). None of them seems to be very convincing. The most plausible one was based on recent simulations by Governato et al. (2012) in which they showed that the dark matter density profile can become flatter (less concentrated) if a large amount of energy from supernovas is able to blow large amounts of gas from the centre of a small subhalo. Nevertheless, the small stellar content of the MW dSphs indicates that this mechanism is not effective in this case. We have also shed some light into this interesting discussion using the CLUES simulations. Di Cintio et al. (2013) have analysed the density profiles of dark matter in subhalos of the LG64-3 and LG64-5 DM and SPH CLUES simulations (see Table A.4) and concluded that the Einasto profile (eq. 3) give a good fit both for subhalos in the DM and SPH simulations.

Our conclusions are slightly different than in Boylan-Kolchin et al. (2011), which were based on assuming NFW density profiles. We find that an Einasto profile with shape parameter  $1.6 \leq n_e \leq 5.3$  provides an accurate matching between simulations and observations, alleviating the massive failure problem first addressed in Boylan-Kolchin et al. (2011). However, in a follow-up paper by the same authors (Boylan-Kolchin et al., 2012), the direct particle data from the Aquarius simulations were used with no appeal to a specific fit of the profiles and they confirmed their previous results. Nevertheless, as shown in the previous reference and, more recently, by Vera-Ciro et al. (2013), a very good agreement with observation is attained considering that the mass of the MW is smaller than  $10^{12} M_{\odot}$ . In our WMAP3 CLUES simulations we have slightly lower masses for MW and M31 ( $5.5 - 7.5 \times 10^{11} M_{\odot}$ ). This would also reduce the probability of

the MW hosting two satellites as bright as the LMC and SMC. Our Galaxy is in fact a rare one. Different studies using the Sloan Digital Sky Survey (SDSS) have concluded that only  $\sim 3.5\%$  of the MW-like galaxies have two satellites as big as the Magellanic Clouds (e.g. Tollerud et al., 2011). On the other hand, a low mass MW would be in conflict with results from abundance-matching based relations between halo mass and stellar mass (see e.g. Behroozi et al., 2013), direct measurements of the MW's virial mass from kinematic studies of its satellites (Boylan-Kolchin et al., 2013), or the recent measurement of the MW's escape velocity from the RAVE survey (Piffl et al., 2013).

Therefore, due to the problems than  $\Lambda$ CDM faces to explain the satellite population in the LG, the view has turned into alternative models of dark matter in which either the short scale power is suppressed because of free streaming, assuming that the mass of the DM particles is in the keV regime (WDM) or the dark matter is self-interacting, producing substructures with cored profiles that can then easily be destroyed (e.g., Vogelsberger et al., 2012; Rocha et al., 2013).

WDM is an attractive alternative to CDM. The power spectrum of DM fluctuations has a sharp cutoff at short scales due to the effect of the thermal velocities of the DM particles when they became non relativistic. For the common assumption of WIMPS as DM candidate, their masses are in the GeV scales and thus, the relic thermal velocities of those particles are very small during the epoch of structure formation. If instead a keV mass particle DM candidate is considered, as the sterile neutrino (e.g. Asaka and Shaposhnikov, 2005), the thermal velocities are sufficiently large to erase, due to free streaming, all perturbations below galactic scales. In Fig 12 we show a comparison between the CDM and WDM power spectra for the case of a  $m_{WDM} = 1$  and 3 keV. On scales much larger than the cutoff, structure formation proceeds very similar in both models, except for the case that there is a delay in the formation of WDM structures with respect to CDM. This translates into smaller fluctuations at high redshift than can be constrained by comparing with astronomical observations of the Lyman  $\alpha$  forest (e.g. Viel et al., 2013).

WDM halos of a Milky Way type size have been recently simulated with high resolution both with collisionless N-body simulations (e.g., Lovell et al., 2013) as well as with radiative gasdynamical simulations (e.g. Herpich et al., 2013)). In our CLUES project we have also done the same experiments but focusing on the formation of the LG as a system of 3 main galaxies (LG64-3-WDM and LG64-3 CDM simulations of Table A.4). A comparison of the dark matter distribution of the LG group in the two models, CDM and WDM (1 keV), at  $z = 0$  can be seen in Fig. 6. A detailed comparison of the internal properties of the main halos in these two models has been published recently in Libeskind et al. (2013a) and we refer the reader to this publication for further information. Here we just want to report a summary of our findings. As can be clearly seen in Fig 6, the two LG groups are in a different stage of evolution. The CDM LG is collapsing and more compact, the WDM LG is dynamically younger, more diffuse and is still expanding. This delay in the evolution implies that WDM halos are smaller than their CDM counterparts at  $z=0$ . They also show lower baryon fractions in their inner parts, where baryons dominate, as compared with CDM. The cutoff in the power spectrum also affects the baryonic processes in non trivial way: from the star formation rates, to the bulge/disk ratios to colours of satellites. In general, the WDM dwarf satellites tend to be less gas rich and less concentrated. We also find marginal evidence of a thickening of the disk gas in one of our WDM galaxies as compared with their CDM counterpart, but this cannot be extrapolated as a general behaviour of disk formation in WDM. The model used in the CLUES simulations (1 keV WDM particle mass) is on the low side of the allowed values imposed by high-redshift Lyman  $\alpha$  constrains (2 – 3 keV). For higher masses of WDM particles, ( $m_{WDM} > 2$  keV) the effects on disk formation have a minor impact (Herpich et al., 2013).

So, we have seen how the LG can be considered as a dark matter laboratory, not only because it is our place in the universe in which we can try to detect the nature of dark matter (either by direct experiments on Earth or from indirect detection of their annihilation/disintegration remnants), but also by comparing astronomical observations of LG galaxies with the predictions of numerical simulations in different dark matter scenarios. We will continue with this issue in section 7 in which we will go a step forward in scale and will show how the observations of the Local Universe can also help us in constraining the nature of dark matter.

## 4. Formation of the Local Group and Local Group - like Objects

### 4.1. The Mass Aggregation History

The issue of how typical is the LG compared with similar objects in the universe is arguably one of the most interesting questions that can be asked within the framework of Near-Field Cosmology. Or, rephrasing it, is the LG typical enough that one can learn from it about the universe at large, thereby making the study of the near field a subfield of cosmology. Forero-Romero et al. (2011) have opted to address the following aspect of the question. Namely, given the present epoch dynamical constraints on the LG, to what extent the mass accumulation history (MAH) of the LG is typical? This has been tested by constructing ensembles of LG-like objects in a suite of 3 different CLUES LG64-5 DM simulations (Table A.4) and the unconstrained BOLSHOI simulation (Klypin et al., 2011), which is used to provide the framework within which the question of 'how typical' is asked.

A numerical study of the LG should start with identifying the main relevant observational features of the LG which will serve as the basis for constructing an ensemble of LG-like objects. Forero-Romero et al. (2011) used DM-only simulations to construct such an ensemble and therefore considered only the dynamical properties of the LG and its environment. The set of criteria used in these studies includes the mass of the two main halos of the LG-like objects, their isolation, proximity to a Virgo-like halo, the distance between the two and the fact that they approaching one another (for a more detailed description see Forero-Romero et al., 2011).

Three different ensembles have been constructed out of the constrained simulations (combined) and separately out of the BOLSHOI simulation. The ensemble of individual halos consists of all haloes in the mass range  $(0.5-5) \times 10^{12} h^{-1} \text{Mpc}$ . The ensemble of pairs, where two halos,  $H_A$  and  $H_B$ , from the *Individuals* sample are considered a pair if and only if halo  $H_B$  is the closest halo to  $H_A$  and vice versa. Furthermore, with respect to each halo in the pair there cannot be any halo more massive than  $5.0 > 10^{12} h^{-1} \text{M}_\odot$  closer than its companion. The sample of isolated pairs is of all pairs which obey also the environmental criteria for a LG-like object. Hence this is the ensemble of LG-like objects. In addition, the select group of the 3 simulated LGs of each one of the constrained simulation forms a sample by itself.

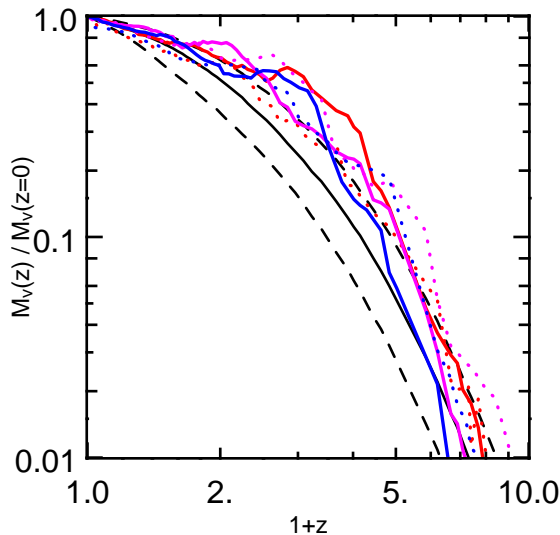


Figure 7: Mass assembly histories of LG halos in the LG64-5 CLUES simulation as a function of redshift. The solid black line shows the median MAH for all halos in the CLUES simulations within the mass range  $5.0 \times 10^{11} h^{-1} \text{M}_\odot < M_h < 5.0 \times 10^{12} h^{-1} \text{M}_\odot$ , the dashed lines show the first and third quartiles. Also plotted as colour lines are the MAHs for the MW (dotted) and M31 halos (continuous) in the three constrained simulations. The assembly history for the LG halos is systematically located over the median values as sign of early assembly with respect to all halos in the same mass range. (Figure taken from Forero-Romero et al. (2011).)

The MAH of the selected halos is defined by three characteristic times, extracted from the merger trees of the halos. The times, measured as look-back time in Gyr, are: a) **Last major merger time** ( $\tau_M$ ), defined as the time when the last FOF halo interaction with ratio 1:10 starts. This limit is considered to be the mass ratio below which the merger contribution to the bulges is  $< 5\%$ - $10\%$  (Hopkins et al., 2010). b). **Formation time** ( $\tau_F$ ) marks the time when the main branch in the tree reached half of the halo mass at  $z = 0$ . This signals the epoch when half of the galaxy mass (gas and stars) is already in place in a single collapsed object. c). **Assembly time** ( $\tau_A$ ): defined as the time when the mass in progenitors more massive than  $M_f = 10^{10}h^{-1}M_\odot$  is half of the halo mass at  $z = 0$ . This time is related to the epoch of stellar component assembly, as the total stellar mass depends on the integrated history of all progenitors (Neistein et al., 2006; Li et al., 2008). The exact value depends on  $M_f$ , and the specific value selected in this work was used to allow the comparison of assembly times against the results of the BOLSHOI simulation which has a lower mass resolution.

The MAH of the three simulated LGs, drawn from the CLUES zoom simulations, is presented by Fig. 7, which shows the actual MAH of these objects. The figure shows also the median and the first and third quartiles of the MAH for all halos in the CLUES simulations within the mass range  $5.0 \times 10^{11}h^{-1}M_\odot < M_h < 5.0 \times 10^{12}h^{-1}M_\odot$ .

Fig. 8 provides the essence of the analysis. It shows the joint distribution of the three MAH times of the different samples. Two basic facts immediately emerge here. One, the 3 simulated LGs show a remarkable clustering in the joint phase space of the MW and M31 MAH characteristic times. This fact is not trivially expected from the selection and construction of the simulated LGs. The other is the distributions from the *Pairs* and *Isolated Pairs* control samples are basically indistinguishable. In other words, detailed selection criteria for halo pairs, based on isolation only, do not narrow significantly the range of dark matter halo assembly properties.

The main finding of Forero-Romero et al. (2011) is that the three LGs share a similar MAH with formation and last major merger epochs placed on average  $\approx 10 - 12$  Gyr ago. Roughly 12% to 17% of the halos in the mass range  $10^{11}h^{-1}M_\odot < M_h < 5 \times 10^{12}h^{-1}M_\odot$  have a similar MAH. In a set of pairs of halos with similar characteristics as the LG, a fraction of 1% to 3% share similar formation properties as both halos in the simulated LG. An unsolved question posed by our results is the dynamical origin of the MAH of the LGs. The isolation criteria commonly used to define LG-like halos do not reproduce such a quiet MAH, nor does a further constraint that the LG resides in a low density environment. The quiet MAH of the LGs provides a favourable environment for the formation of disk galaxies like the MW and M31. The timing for the beginning of the last major merger in the Milky Way dark matter halo matches with the gas rich merger origin for the thick component in the galactic disk. Our results support the view that the specific large scale environment around the Local Group has to be explicitly considered if one wishes to use near field observations as validity test for  $\Lambda$ CDM.

#### 4.2. The kinematics of the Local Group in a cosmological context

Recent observations constrained the tangential velocity of M31 with respect to the MW to be  $v_{M31,tan} < 34.4 \text{ km s}^{-1}$  and the radial velocity to be in the range  $v_{M31,rad} = -109 \pm 4.4 \text{ km s}^{-1}$  (van der Marel et al., 2012). This has motivated Forero-Romero et al. (2013) to revisit the question of how typical is the LG with respect to new kinematical data, using the simulations and selection of objects of Forero-Romero et al. (2011). The following main findings have emerged. The most probable values for the tangential and radial velocities in these pairs are  $v_{rad,\Lambda\text{CDM}} = -60 \pm 15 \text{ km s}^{-1}$  and  $v_{tan,\Lambda\text{CDM}} = 50 \pm 5 \text{ km s}^{-1}$ . Using the same absolute values for the uncertainty in the observed velocity components, halos within the preferred  $\Lambda$ CDM values are found to be five times more common than pairs compatible with the observational constraint. The qualitative nature of these results is still valid after a narrower selection on separation and total pair mass. Additionally, pairs with a fraction of tangential to radial velocity  $f_t < 0.32$  (similar to observations) represent 8% of the total sample of LG-like pairs. Making a tighter selection to match the observational constraints on the separation and total mass results in zero pairs compatible with observations.

Approximating the LG as two point masses the above mentioned results are expressed in terms of the orbital angular momentum  $l_{orb}$  and the mechanical energy  $e_{tot}$  per unit of reduced mass. Uncertainties in the tangential velocity, the square of the norm of the velocity and the total mass in the LG lead to poorer

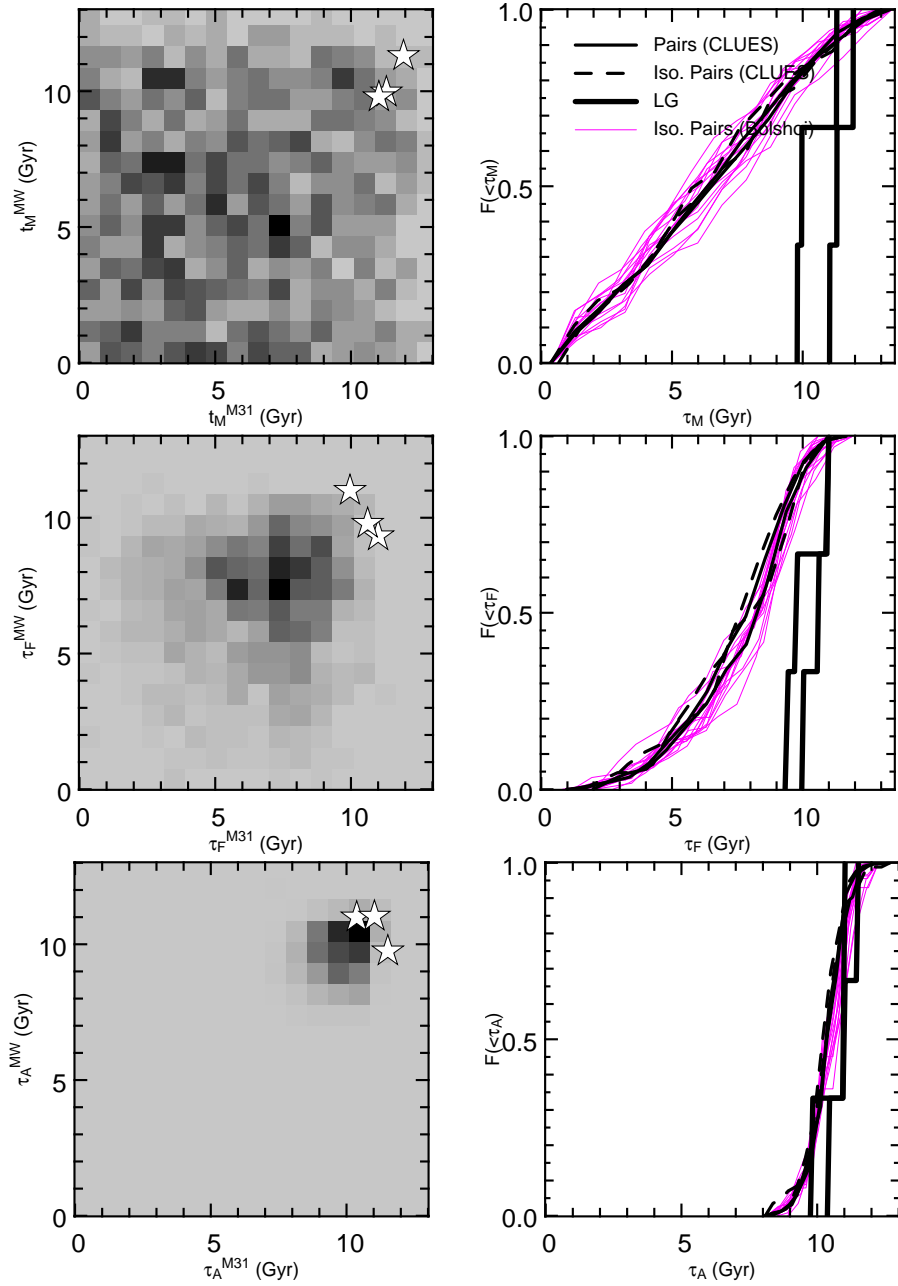


Figure 8: *Left column.* Joint distributions of three different times (last major merger, formation and assembly) describing the mass aggregation histories. Each point in the plane represents a pair MW-M31 with histories described by the time values at that point. Levels in shading coding indicate the number of halo pairs in the BOLSHOI simulations in that parameter range. The stars mark the location of the three LG pairs from the constrained simulations. *Right column* Integrated probability of these three different times. The continuous black lines represent the results for the *Pairs* sample in the CLUES simulations. The *Isolated Pairs* sample from CLUES is represented by the thick dashed lines. The results from the *Isolated Pairs* samples in eight sub-volumes of the BOLSHOI simulation are represented by the thin continuous grey lines. The thick continuous lines represent the results for the *LG* sample. (Figure taken from Forero-Romero et al. (2011).)

constraints on the number of simulated pairs that are consistent with the observations. Nevertheless, in the case of the LG-pair sample that also fulfills the separation and total mass criteria there is a slight tension between simulation and observation.

The kinematics of the three simulated LGs is dominated by radial velocities. However their velocity components differ from the observational constraints while their mechanical energy and orbital angular momentum are in broad concordance with observations. There is only one pair that fulfills all the separation, total mass constraints and matches the most probable value for the dimensionless spin parameter  $\lambda$  inferred from observations. LG-like pairs in  $\Lambda$ CDM show preferred values for their relative velocities, angular momentum and total mechanical energy. The values for the orbital angular momentum and energy, merged into the  $\lambda$  spin parameter, are in mild disagreement with the observational constraints. However, there is a strong tension with the precise values for the radial and tangential velocities. This leads to an interesting observation, assuming, in a very rough approximation, that the mechanical energy and total orbital angular momentum of the LG are conserved, as in the classical two-body problem. Then the consistency of the energy and orbital angular momentum of the simulated LGs with the observed one, and the inconsistency with respect to the actual values of the radial and tangential velocities, implies that the observed LG started from initial conditions that are not captured by the simulated LGs. The unique phase of the LG on its orbit is not reproduced by the simulations reported here.

## 5. Weighting the Local Group

The estimation of the mass, be it the total, DM or the baryonic mass, of cosmological objects such as galaxies, haloes, groups and clusters of galaxies, is a very challenging task. In many ways the problem is an ill defined one. The cosmological structures mentioned here are not isolated and are not well separated from the continuous mass distribution in the universe. This is also valid in the theoretical domain, where mass estimation is unaffected by observational limitations. Yet, algorithms are defined and halo finders are devised so as to provide mass estimators which conform with theoretical understanding and observational feasibility (see Knebe et al., 2013a,b, and references there in).

The CLUES simulations provide a unique numerical laboratory for testing mass estimators designed to assess the mass of very local objects of interest, such as the the MW and M31 galaxies, nearby satellites and dwarf galaxies and the LG as an object by itself.

### 5.1. Mass estimation by the Timing Argument

It has been known for a long time that the total mass of the LG can be estimated by assuming it to be a two-body system, i.e. an isolated system made of two point mass particles whose individual masses do not change with time. A further assumed simplification is that the two galaxies formed at the time of the Big Bang at zero distance, hence their orbital angular momentum is zero. The so-called “mass estimation by the timing argument” is based on the fact that in the above simplified model the age of the universe, the distance between the MW and M31 and their relative velocity determine the total mass of the two objects, and it can be easily calculated (Kahn and Woltjer, 1959; Lynden-Bell, 1981). A naive examination of the model would cast serious doubts on the ability of the model to produce a useful prediction of the mass. The LG is not an isolated system, the orbital angular momentum of the two galaxies is not necessarily zero, the two galaxies and their halos are not point-like particles, and their masses certainly change over their dynamical evolution. It is therefore not surprising that the mass estimation by the timing argument (TA) has not played a prominent role in the effort to determine the mass of the LG. Kroecker and Carlberg (1991) and Li and White (2008) took the steps towards calibrating the model and make it into a quantitative tool. The calibration consists of identifying LG-like pairs of halos in large scale cosmological simulations and applying the TA mass estimator to these objects.

The CLUES has been used for testing the TA mass estimation<sup>3</sup>. That study consists of analysing a suit of the Box64-3 and three different realizations of Box64-5 DM only simulations (see Table A.3), construction of

---

<sup>3</sup>Shalhevet Bar-Asher, 2011, MSc. Thesis, Hebrew University, unpublished

Simulation	# of pairs	25%	50%	75%	$\frac{\Delta\eta}{\eta}$
Box64-3	14	0.80	1.40	1.90	0.29
Box64-5, A	9	1.28	1.36	1.81	0.19
Box64-5, B	23	1.35	1.83	2.81	0.40
Box64-5, C	13	1.06	1.46	1.90	0.29
Box64-5, all	45	1.23	1.55	2.03	0.26
L&W	16479	1.07	1.48	2.12	0.35

Table 1: The  $\eta_{vir}$  percentile values for the Box64-3 the three Box64-5 CLUES simulations, the distribution for the three Box64-5 simulations combined. The last row shows the results of Li and White (2008) and are presented for reference.

an ensemble of LG-like objects, following the selection criteria outlined in §4.1. Each one of the simulations harbours a “good LG” at its centre, namely a simulated objects which obeys all the selection criteria for being considered as a numerical counterpart of the observed LG. Here the mass by the TA is compared with the virial mass of the LG, namely the sum of the virial masses of the two most massive members of the LG-like object. Table 1 shows the number of LG-like objects in each simulations, the median and the 25% and 75% quartiles of the distribution of  $\eta_{vir}$ , the ratio of the virial masse of the LG-like object to the mass estimated by the TA ( $\eta_{vir} = M_{vir}/M_{TA}$ ). The table shows also the results obtained by Li and White (2008) as reference. One should note here that the later study is based on the  $\Lambda$ CDM cosmology but with a different set of cosmological parameters and a different selection of simulated LG-like objects than those reported here.

The results presented here are consistent with the findings of Li and White (2008), with a median value of  $\eta_{vir}$  of about 1.5, but with a smaller scatter. It follows that the TA systematically biases the estimated mass towards smaller than the actual virial mass. Adopting the following parameters for the LG, an infall velocity of  $130 \text{ km s}^{-1}$ , a distance of  $0.784 \text{ Mpc}$  and assuming the WMAP5 age of the universe of  $13.75 \text{ Gyr}$ , we find  $M_{TA} = 5.3 \times 10^{12} M_{\odot}$ . The calibration from TA mass estimation to the virial mass yields  $M_{vir} = (8.2^{+2.5}_{-1.6}) \times 10^{12} M_{\odot}$ . The error bars reflect the theoretical uncertainties in the  $M_{TA} - M_{vir}$  relation, which are much larger than the observational uncertainties, which are therefore ignored here.

### 5.2. Mass estimation by the Timing Argument in the presence of dark energy

The classical TA model is formulated within a cosmological model that ignores the presence of a dark energy (DE) component (Kahn and Woltjer, 1959; Lynden-Bell, 1981). Yet, a DE component changes the time behaviour of the background universe, and hence is expected to affect the TA model. This has been recently considered by Partridge et al. (2013). In Newtonian terms the DE is acting to provide an effective repulsive force, and therefore the modified TA model is expected to result in a higher estimated mass. Using the latest compilation of cosmological parameters of the PLANCK CMB experiment the modified TA model yields  $M_{TA} = (4.73 \pm 1.03) \times 10^{12} M_{\odot}$ , an estimation which is 13% higher than the original TA model (Partridge et al., 2013). A calibration of the modified TA model by the sample of LG-like objects (reported in §5.1) yields  $M_{vir}/M_{TA} = 1.04 \pm 0.16$ . Applying it to the TA mass of the LG results in an estimated virial mass of  $M_{LG} = (4.92 \pm 1.08(\text{obs.}) \pm 0.79(\text{sys.})) \times 10^{12} M_{\odot}$  (Partridge et al., 2013).

### 5.3. Mass Estimators of the MW and M31 Galaxies

Gas rotation curve data provide a reliable estimation of the mass distribution within the innermost few tens of kiloparsec, of both the MW and the M31 galaxies, but estimation of the mass out to the virial radius needs to rely on the kinematics of a tracer populations. These tracers can either be globular clusters, halo stars or satellite galaxies or a combination of these. Earlier efforts in that direction include the mass of four MW dwarf spheroidals (dSphs) satellites that were constrained with high precision by kinematic data sets (Lokas, 2009). Line-of-sight kinematic observations enable accurate mass determinations at half-light radius for spherical galaxies such as the MW dSphs (Wolf et al., 2010): at both larger and smaller radii, however, the mass estimation remains uncertain because of the unknown velocity anisotropy.



The mass estimation of our own Galaxy, the MW, is about to be revolutionized by the upcoming data of the space mission GAIA which will provide full six-dimensional phase-space information for all objects, in the nearby universe, brighter than  $G \approx 20$  mag. GAIA’s mission is to create the largest and most precise three dimensional chart of the Milky Way by providing precise astrometric data like positions, parallaxes, proper motions and radial velocity measurements for about one billion stars in our Galaxy and throughout the LG.

Anticipating the GAIA upcoming data and a situation at which the position and proper motion data of satellite galaxies of the MW will be available, Watkins et al. (2010) suggested a suit of “scale-free projected mass estimators” to calculate the mass of the MW. The estimators are based on simplifying assumptions such as spherical symmetry and a scale-free density profile, which constitute only a proxy to the actual MW. This motivated Di Cintio et al. (2012) to test Watkins et al. (2010) mass estimators against the simulated MW and M31 of the CLUES LG64-5 high resolution zoom simulation. It was shown before that the considered mass estimators work rather well for isolated spherical host systems, and this was extended by Di Cintio et al. (2012) to examine their applicability to the MW and M31 haloes that form a binary system with a distinct satellite population. Their analysis consists of the application of the mass estimators using a number of sub-haloes similar to the number of observed satellites of MW and M31,  $N \sim 30$ , with the same mass range and following the same observed radial distribution. It has confirmed the notion that the scale-free estimators work remarkably well – even in our constrained simulation resembling a realistic numerical model of the actual Local Group (as opposed to isolated MW-type haloes considered in other works). It has further validated that the accuracy increases when the full phase-space information of the tracer objects is assumed. The study has demonstrated, in the isotropic case, that no further assumptions are required with respect to the host’s density profile: under the assumption that the satellites are tracking the total gravitating mass the power-law index  $\gamma$  derived from the radial satellite distribution  $N(< r) \propto r^{3-\gamma}$  is directly related to the host’s mass profile  $M(< r) \propto r^{1-\alpha}$  as  $\alpha = \gamma - 2$ ; it has been shown that utilizing this relation for any given  $\gamma$  will lead to highly accurate mass estimations within our numerically modelled LG. This is a fundamental point for observers and the applicability of the scale-free mass estimators, respectively, since the mass profile of the MW and M31 haloes is not a priori known. Although future missions will improve the census of satellite galaxies, it has been asserted that mass estimators of the type studied by Watkins et al. (2010) can already be safely applied to the real MW and M31 system, and will acquire even more importance with the forthcoming GAIA data.

## 6. Dark Matter distribution in the Local Universe: The Cosmic Web

The translation of the vivid visual impression of the cosmic web into a quantitative mathematical formalism poses an intriguing challenge. There are two basic approaches to the problem. One is observationally motivated, and it essentially aims at defining the web from the point distribution presented by the observed galaxy distribution (Lemson and Kauffmann, 1999; Novikov et al., 2006; Aragón-Calvo et al., 2007; Sousbie et al., 2008). The other approach is motivated by the theoretical quest to understand the emergence of the cosmic web and it is more applicable to numerical simulations rather than observational redshift surveys (Hahn et al., 2007; Forero-Romero et al., 2009). The V-web web finder, which follows the later approach, is based on Clouds-in-Cells (CIC) interpolating the velocity shear tensor on a grid, and calculating the number of the velocity shear tensor eigenvalues above a certain threshold. The number of eigenvalues above a threshold determines the web type of a given cell on the grid. The V-web finder has two free parameters which determine the web, the Gaussian smoothing of the CIC gridded fields (density, velocity, etc.) and the threshold for the eigenvalues of the (normalized by the Hubble constant) velocity shear tensor (Hoffman et al., 2012; Libeskind et al., 2012, 2013b).

The BOX64-5 DM-only simulation (see Table A.3) is used here as a proxy to the actual nearby LSS. The simulation contains a simulated LG-like at the centre of the computational box. The analysis focuses first on the DM distribution and the cosmic web properties of the full computational box and then it zooms to study the properties and structure of the web in the immediate neighbourhood of the LG. A Gaussian kernel smoothing of  $R_s = 0.25h^{-1}\text{Mpc}$  and a dimensionless threshold of 0.45 are used to determine the V-web.

web elements	volume filling fraction	mass filling fraction
voids	0.68 (0.69)	0.13 (0.15)
sheets	0.27 (0.26)	0.36 (0.37)
filaments	0.046 (0.046)	0.34 (0.37)
knots	0.0036 (0.0035)	0.17 (0.11)

Table 2: The volume and mass filling factors of the various web elements. The filling factors obtained without the multi-scale correction are given in the parentheses.

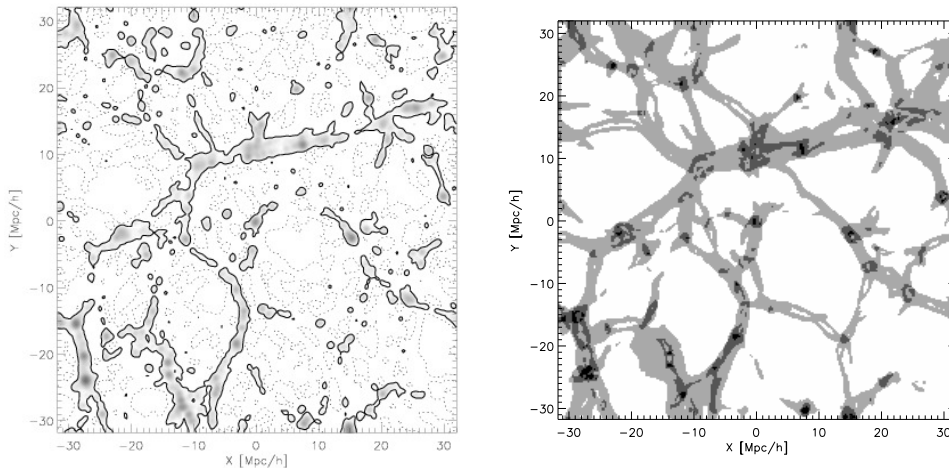


Figure 9: The normalized density field and the cosmic web, based on the CIC density field of the full computational box (BOX64) spanned on a  $256^3$  grid and Gaussian smoothed on the scale of  $0.25h^{-1}\text{Mpc}$ : a. The density field presented by  $\log \Delta$  (grey scale correspond to overdense and dashed contours to under-dense regions. The solid contour represents the mean density. (upper-left panel). b. The velocity based cosmic web generated with  $\lambda_{th}^V = 0.44$  made of voids (white), sheets (light grey), filaments (dark grey) and knots (black). Note that the map presents a planar cut through the cosmic web, hence sheets appear as long filaments and filaments as isolated compact regions. (Figure taken from Hoffman et al. (2012).)

### 6.1. The Local Dark Matter Distribution and the Cosmic Web

Fig. 9 presents the normalized density,  $\Delta$ , field and the cosmic web of the simulated Supergalactic Plane, where  $\Delta = \rho/\bar{\rho}$  and  $\bar{\rho}$  is the cosmological mean density. The left panel shows the logarithm of the normalized density field and the right one exhibits the corresponding cosmic web. Both the density field and web are based on the CIC gridded and smoothed with a Gaussian kernel of  $0.25h^{-1}\text{Mpc}$  fields.

Both panels of Fig. 9 show a two dimensional cut in a three dimensional computational box, hence the filamentary-like looking structures that dominate the density map and the cosmic web are actually sheets that are bisected by the Supergalactic Plane. Most of the actual filaments appear in these two-dimensional maps as compact knots. The LG is located within a compact knot (black compact region in the web map), embedded in a filament that runs perpendicular to the Supergalactic Plan. The LG neighbourhood, up to a distance of about  $15h^{-1}\text{Mpc}$  is dynamically dominated by the Local Supercluster, a structure that harbours the simulated Virgo and Ursa Major clusters. The LG itself resides within an under-dense region, characterized as a void by the V web finder, bisected by the sheet, that contains the filament that contains the LG.

Table 2 present the mass and volume filling factors of the voids, sheets, filaments and knots of the full computational box. The table shows that while most of the volume of the box is taken by the voids, the sheets and filaments contain about a third of the total mass of the box, with the rest spreads almost evenly between the voids and knots. The threshold which defines the V-web has been chosen so as to match

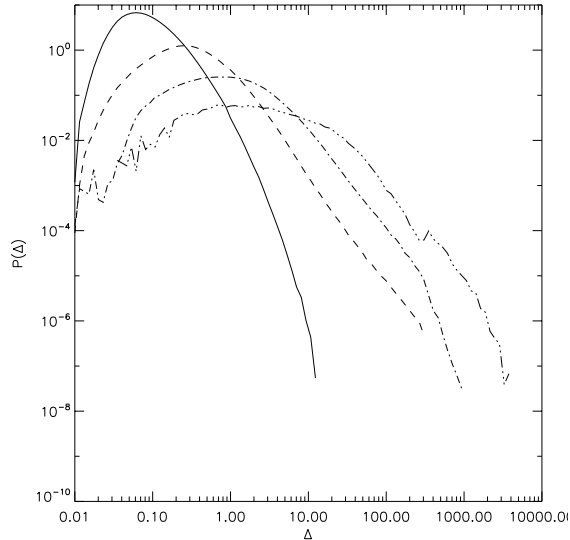


Figure 10: The probability distribution of grid cells as a function of the fractional density,  $P(\Delta)$ , is plotted for the various V-web elements, voids (full line), sheets (dashed), filaments (dot-dashed) and knots (dot-dot-dashed). (Figure taken from Hoffman et al. (2012).)

the visual inspection of the simulation (see Hoffman et al. (2012)). This threshold roughly divides the mass distribution into two halves, namely the mass filling factors of voids and sheets combined, and of the filaments and knots combined are roughly equal,  $\approx 0.5$ .

Fig. 10 shows a histogram by CIC cells of the normalized density field for the different web elements. The histogram shows the relative abundance of CIC cells as a function of their (normalized) density. It clearly shows that although there is a strong correlation of the density of a CIC cell with its web type there is no one-to-one correspondence between the web classification and the density.

## 6.2. The Local Group and the Cosmic Web

Fig. 11 zooms in the inner part of the computational box and shows the density field, the cosmic web and the DM halos in the immediate vicinity of the simulated LG. The plot shows the three principal Supergalactic planes within a box of a side length of  $8h^{-1}\text{Mpc}$  centred on the LG. The filled circles represent the DM halos, with colour representing the web classification and the size of symbol scaling with halo mass. The two most massive halos, located at the centre of the zoom box, are the simulated MW and M31 halos. At the centre of the box there is a small, i.e. an effective radius of roughly  $\approx 0.5h^{-1}\text{Mpc}$ , blob classified as a knot. This is the numerical counterpart of the LG, with the centre of the simulated MW and M31 halos lying just outside the knot, but having a good part of their mass embedded in the knot. The simulated group is located within a filament that runs perpendicular to the Supergalactic Plane, and is close to coincide with the SGZ axis. As described above, that filament is embedded within a sheet that is also running perpendicular to the Supergalactic Plane.

## 7. The Local Universe as a Dark Matter Laboratory

§3.1 shows how observations of galaxies in the LG can be used to constrain the nature of DM. The number of low mass satellites of MW and M31 as compared with CDM predictions can be explained through the effects of gasdynamics on baryons, making them invisible, or they can simply not exist, if DM particles have a mass in the keV scale. The nature of the DM affects also the abundance and distribution of isolated dwarf

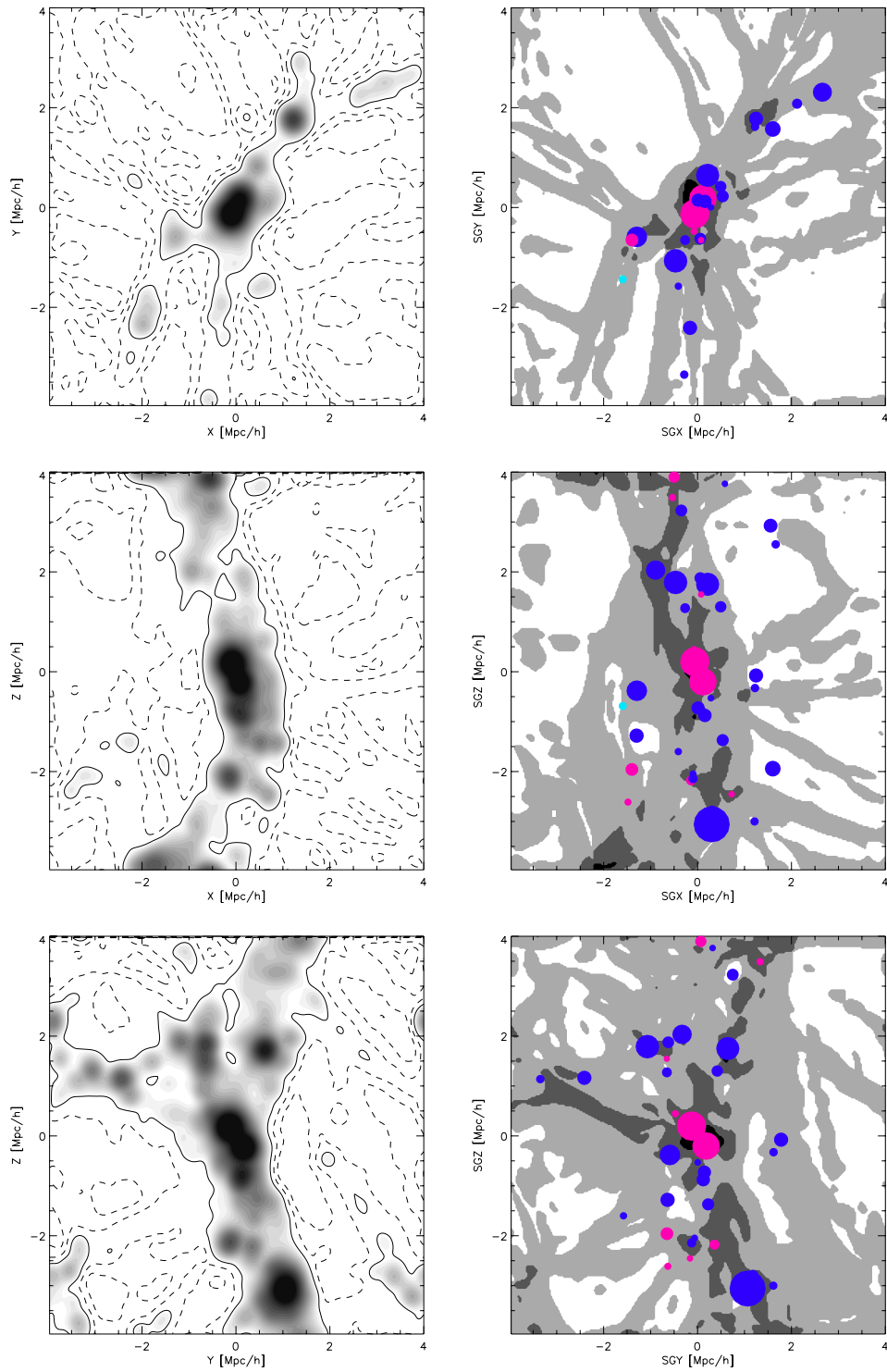


Figure 11: A zoom on the simulated LG in the BOX64-5 DM-only simulation. The logarithm of the fractional density,  $\Delta$ , (left column) and the C-web (right column) of the three principal planes are shown. The contour coding of Figure 9 is followed here. The filled coloured circles represent DM halo, with the radii of circles scaling linearly with the halos' virial radius, and the colours correspond to the web classification (cyan - sheets, blue - filaments, red - knots).

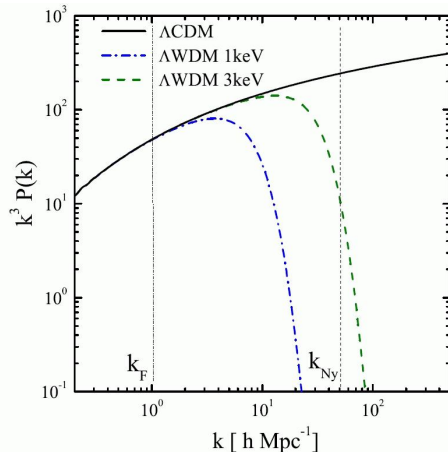


Figure 12: Dimensionless power spectra of a cosmological model with CDM (solid black line) and WDM (blue and green dashed lines). (Figure taken from Tikhonov et al. (2009))

galaxies and the Local Universe provides the optimal test site for confronting models with observations of such galaxies. The present section presents the comparison of predictions based on CDM and WDM full box Box64-3 CLUES simulations (Table A.3) with observations of the distribution of dwarf galaxies.

Fig. 12 shows the underlying primordial power spectrum of the  $\Lambda$ CDM and  $\Lambda$ WDM models. Two cases of the WDM scenario are shown, with a mass of the DM particles of 1 and 3 keV. We assumed a very low dark matter mass of 1 keV which is a lower bound set by observations (see the discussion in Zavala et al., 2009; Tikhonov and Klypin, 2009). The 1 keV mass corresponds to the maximal impact the WDM model can have on structure formation. Same initial conditions are used in the CDM and WDM simulations, modulated by their different power spectra.

### 7.1. The size of mini-voids in the Local Volume

The Hubble Space Telescope observations have provided distances to many nearby galaxies which are measured using the tip of the Red Giant Branch (TRGB) stars. Special searches for new nearby dwarf galaxies have been undertaken by Karachentsev et al. (2004). The distances of these galaxies in the Local Volume are measured independently of redshifts. Therefore, we know both their true 3D spatial distribution and their radial velocities. The distances have been measured with accuracies as good as 8 – 10%. Tikhonov and Klypin (2009) have used these observational data to construct the spectrum of observed mini-voids in the Local Volume ( $\sim 10$  Mpc around LG). They came to the conclusion that the observed spectrum of mini-voids can be only explained if one assumes that objects with  $V_c > 35$  km s $^{-1}$  define the local mini-voids and these objects host galaxies brighter than  $M_B = -12$  (see the right hand side of Fig. 13). The CDM CLUES simulation predicts almost 500 haloes with  $20 < V_c < 35$  km s $^{-1}$  within the mini-voids in the Local Volume. However only 10 quite isolated dwarf galaxies have been observed with magnitudes  $-11.8 > M_B > -13.3$  and rotational velocities  $V_{rot} < 35$  km s $^{-1}$  which points to a similar discrepancy as the well known predicted overabundance of satellites. In the WDM model, on the other hand, the truncated power spectrum of the WDM model suppresses the formation of galaxies in small mass halos. Thus, in the WDM CLUES simulation, the observed spectrum of mini-voids can be naturally explained if DM haloes with circular velocities larger than  $\sim 15 - 20$  km s $^{-1}$  host galaxies, as can be clearly seen in the left panel of Fig. 13. The interested reader is referred to Tikhonov et al. (2009) for further details.

### 7.2. The abundance of HI galaxies in the Local Universe

Zavala et al. (2009) compared the velocity function measured from the Arecibo Legacy Fast ALFA (ALFALFA) survey (Giovanelli et al., 2005) with the velocity function derived from the Box64-3 CDM

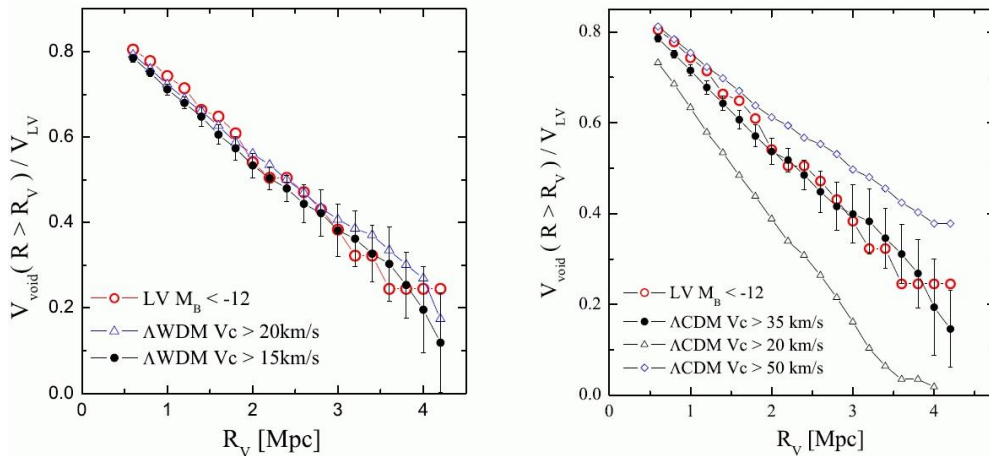


Figure 13: Right: The spectrum of mini-voids in the observational sample with  $M_B < -12$  (red circles) is compared with the spectrum of mini-voids in a halo sample with circular velocity  $V_c > 20 \text{ km s}^{-1}$  (open triangles),  $V_c > 50 \text{ km s}^{-1}$  (open diamonds), and  $V_c > 35 \text{ km s}^{-1}$  (filled black circles) obtained from Box64-3 CDM simulation. Left: The same in the Box64-3 WDM simulation but for a halo sample with circular velocity  $V_c > 20 \text{ km s}^{-1}$  (open blue triangles) and  $V_c > 15 \text{ km s}^{-1}$  (filled black circles). (Figures taken from Tikhonov et al. (2009))

and WDM CLUES simulations. Fig. 14 shows that ALFALFA data exhibits a flattening in the velocity function for low circular velocity galaxies that agrees very well with the predictions of Box64-3 WDM CLUES simulation, while the CDM model present a discrepancy of more than an order of magnitude due to the over-abundance of low velocity halos. This results has been recently confirmed by Papastergis et al. (2011) using an updated, more complete version of the ALFALFA catalogue.

The fact that much more low mass DM halos are predicted by cosmological simulations than low luminosity galaxies are observed can be explained by gas-dynamical processes which prevent star formation in low mass halos, as we have explained in §3.1. Such gas stripping processes are assumed to occur in low mass satellite halos that are inside a more massive parent halo. The fact that also dwarfs in the field are missing (as described in Tikhonov et al. (2009)) is difficult to explain by gas stripping induced by the interaction with their host halos. In Benítez-Llambay et al. (2013) we have shown that a dwarf galaxy moving with high relative speed through a sheet or a filament of the cosmic web is losing a significant fraction of its gas. This new mechanism offers an interesting explanation for the missing dwarf galaxy problem in the Local Volume.

### 7.3. Gamma rays from dark matter annihilation/decay

One of the main motivations for launching the FERMI satellite, that is scanning the whole sky in the gamma ray band, was the possible identification of the nature of DM, assuming it is made of WIMPs. In that case, gamma-rays are generated as secondary products of WIMP decay or annihilation (e.g. Strigari, 2013). In the first case, the gamma production is proportional to the DM density, while in the case of annihilation, it is proportional to the density squared. This would have made the MW centre to be the prime target for looking for DM related signal. However, the galactic centre harbours other sources, of more astrophysical nature, of gamma rays emission, thereby rendering the possible DM-related gamma ray signal very difficult to detect. Other targets to look for indirect signal of DM are the MW satellites and M31. However, no gamma emission from any of the MW satellites has been detected yet by FERMI. Other nearby DM dominated structures, like the Virgo and Coma clusters are the next possible targets for DM detection. This prompted Cuesta et al. (2011) to use the CLUES BOX160 DM-only simulation to compute all-sky simulated FERMI maps of gamma-rays from DM decay and annihilation in the Local Universe, Cuesta et al. (2011) concluded that FERMI observations of nearby clusters and filaments are expected to give stronger constraints on decaying DM compared to previous studies. It was shown, for the first time,

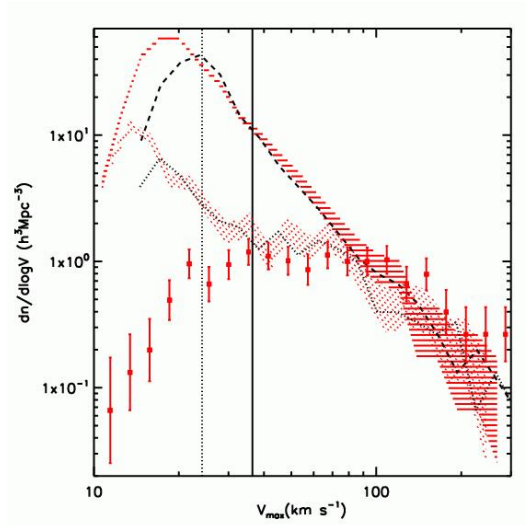


Figure 14: The velocity function of ALFALFA galaxies (square symbols with error bars). Predictions from the CLUES simulations for the same field of view are shown as the dashed ( $\Lambda$ CDM) and dotted (ACDM) red areas. The vertical solid line marks the value of  $V_{max}$  down to which the simulations and observations are both complete. (Figure taken from Zavala et al. (2009))

that the filaments of DM distribution in the Local Universe are promising targets for indirect detection. On the other hand, the prospects for detection of DM annihilating signal from nearby structures are less optimistic even with extreme cross-sections.

Another example of how the simulations of the Local Universe can be used to set constraints to the physical properties of the possible candidates of DM is shown in Gómez-Vargas et al. (2012). Using the BOX160 simulation these authors constructed a simulated whole sky density maps and studied the prospects of the FERMI telescope to detect a monochromatic line of gamma emission due to gravitino decay. The DM halo around the Virgo galaxy cluster was selected as a reference case, since it is associated with a particularly high S/N ratio and is located in a region scarcely affected by the astrophysical diffuse emission from the galactic plane. These authors found that a gravitino with a mass range of  $0.6 - 2$  GeV, and with a lifetime range of about  $3 \times 10^{27} - 2 \times 10^{28}$  sec would be detectable by the FERMI with a S/N ratio larger than 3. They also obtained that gravitino masses larger than about 4 GeV are already excluded by FERMI data of the galactic halo.

## 8. Summary

According to the standard model of cosmology the universe consists mainly of Dark Energy and Dark Matter with a small contribution of baryons. The DM density is about 6 times larger than the baryon density. DM is the main driver of structure formation in the universe, but unfortunately little is known about the nature of the particles which make up the DM. The Local Universe is a very well studied and observed region in which structures on all scales from clusters of galaxies down to the tiniest dwarf galaxies can be observed, and thereby it provides the best possibility for studying DM in an astrophysical context.

The CLUES constitutes a framework for performing numerical cosmological simulation that are constrained to reproduce the Local Universe. “Local” is used here to denote the neighbourhood of the Local Group, extending out to a depth that ranges typically from a very few to a few tens of Megaparsecs. The CLUES is the numerical counterpart of the Near-Field Cosmology, which aims at studying cosmology at large by observing the Local Universe and confronting theories and models of structure formation with local findings. It constitutes a numerical laboratory designed to experiment with structure formation processes in

a way that enables a direct confrontation with the observed Local Universe. The current paper is a report on the first steps taken in this direction.

One of the most exciting challenges that Near-Field Cosmology and the CLUES project are facing is the question of how typical the LG is. To the extent that it can be defined as 'typical' then the study of the LG can shed light on the formation of structure in the universe at large, thus making the study of the near field indeed part of cosmology. In a first attempt to address the problem Forero-Romero et al. (2011) studied the MAH of simulated LGs, chosen so as to reproduce the main dynamical features of the LG and its environment, and compared it with the MAH of similar objects selected from the random BOLSHOI simulation. The main finding of the study is that the simulated LGs have a quiet MAH, with their characteristic mass aggregation look-back times being of the order of 10 Gyrs and thereby statistically significantly longer than those of the random control sample. The interesting point of the MAH study is that the constraints imposed on the initial conditions and on the selection of the LG-like simulated objects are all expressed by present epoch observables. Yet, the LGs that emerge from the simulations are characterized by a long quiescent look-back time, unlike their randomly chosen counterparts. These are preliminary results but they open an interesting window into the mass aggregation history of the LG.

The CLUES simulations have also been used as a DM laboratory. This has been conducted along two different paths. One is the study of the formation of a LG-like object in two cosmological models with CDM and WDM particles. Using same initial conditions, numerical resolution and sub-grid physics models the CDM and WDM simulations were performed and compared. Libeskind et al. (2013a) have recently presented a detailed analysis of the CDM and WDM constrained simulations. Apart from the expected differences with respect to the abundance and distribution of satellites, and their associated baryonic physics, a new interesting result has been found. The two simulated LG-like objects are in different stages of evolution. The CDM LG is beyond its turn-around phase and is more compact. The WDM object, on the other hand is dynamically younger, more diffuse and has not reached turned-around. The interesting aspect of the difference between the two cases is that in spite of the fact that the CDM and WDM power spectra coincide on the scale of the LG, namely for mass scale larger than  $\approx 10^{12}h^{-1}\text{Mpc}$ , they do differ dynamically. It follows that the cross-talk between different scales affects the dynamics on the LG scale. This does not mean, of course, that a proper LG-like object cannot be found in a WDM scenario. But, compared with CDM, it would be less likely to find such an object in an environment constrained to mimic the one in which the LG formed.

The other approach to using the Local Universe as a DM laboratory is by using full box DM-only constrained simulations, assume some simplified model for populating DM halos with galaxies, and then compare the outcome with local surveys of galaxies. By varying the nature of the DM, and hence the power spectrum of the initial condition, while keeping all other aspects of the simulations intact, one can set stringent constraints on the nature of the DM or the model used to associate galaxies with halos. This is the approach adopted by Zavala et al. (2009)) and by Tikhonov et al. (2009). Using, what might be considered a very naive model of associating galaxies with DM halos, the comparison with the observed velocity function of the ALFALFA galaxies (Giovanelli et al., 2005) and the spectrum of mini-voids in the very Local Universe (Tikhonov and Klypin, 2009) clearly favours the WDM model on the CDM one.

CLUES provides a promising way for testing models of galaxy and structure formation within the very Local Universe. The work reported in this paper constitutes only the first steps in that direction. Improved data and more advanced methods of the reconstruction of the primordial initial conditions (Doumler et al., 2013b,c; Heß et al., 2013; Sorce et al., 2013) that seeded the local observed structure are currently being employed by the collaboration. This will result in improved and more tightly constrained simulations which will enable a more thorough experimentation with Near-Field Cosmology in the CLUES numerical laboratory.

## Appendix A. Overview of CLUES simulations

The CLUES collaboration has performed a series of numerical simulations of the evolution of the Local Universe and, in particular, the Local Group. These simulations are performed in different boxes and with different resolutions. There are Dark Matter only simulations as well as simulations with full gas physics,



including cooling, UV photoionization, star formation, Supernovae feedback and galactic winds. A more general overview can be found at the CLUES web page (<http://clues-project.org>). These simulations are publicly available on request. In the following two tables we briefly summarize the simulations performed in a full box (Table A.3) as well as the high-resolution, zoomed-in resimulations of LG objects (Table A.4).

Name of simulation	cosmological model	box size $h^{-1}\text{Mpc}$	number of particles	particle mass $h^{-1}M_{\odot}$
Box160	WMAP3	160	$1024^3$	$2.55 \times 10^8$
Box64-3	WMAP3	64	$1024^3$	$1.64 \times 10^7$
Box64-3-WDM	WMPA3	64	$1024^3$	$1.64 \times 10^7$
Box64-5	WMAP5	64	$1024^3$	$1.84 \times 10^7$

Table A.3: Full box dark matter only simulations performed within the CLUES project. WMAP3 refers to the following set of parameters:  $\Omega_{\Lambda} = 0.76$ ,  $\Omega_{\text{matter}} = 0.24$ ,  $\Omega_{\text{Baryons}} = 0.0418$ , Hubble parameter  $h = 0.73$ , normalization  $\sigma_8 = 0.75$ , slope of the primordial power spectrum  $n = 0.95$ . WMAP5 refers to the following set of parameters:  $\Omega_{\Lambda} = 0.721$ ,  $\Omega_{\text{matter}} = 0.279$ ,  $\Omega_{\text{Baryons}} = 0.046$ , Hubble parameter  $h = 0.7$ , normalization  $\sigma_8 = 0.817$ , slope of the primordial power spectrum  $n = 0.96$ .

Name of simulation	cosmological model	type $h^{-1}\text{Mpc}$	number of particles	DM/stellar particle mass $h^{-1}M_{\odot}$
LG64-3	WMAP3	DM	$4096^3$	$2.55 \times 10^5$
LG64-3	WMAP3	SPH	$4096^3$	$2.22 \times 10^4$
LG64-3-WDM	WMPA3	DM	$4096^3$	$2.55 \times 10^5$
LG64-3-WDM	WMPA3	SPH	$4096^3$	$2.22 \times 10^4$
LG64-5	WMAP5	DM	$4096^3$	$2.87 \times 10^5$
LG64-5	WMAP5	SPH	$4096^3$	$2.37 \times 10^4$

Table A.4: Re-simulations of the the Local Group identified in the simulations (in the box of  $64 h^{-1}\text{Mpc}$  size) listed in Table A.3. The resimulations are performed either as dark matter only simulations (marked as DM) or with hydrodynamics including cooling, star formation and feedback (marked as SPH). WMAP3 and WMAP5 refers to the set of parameters given in Table A.3. The number of particles refers to the formal resolution in the resimulation area (a sphere of radius  $2 h^{-1}\text{Mpc}$  centred at the Local Group). The last column provides the mass of a DM particle (in DM only simulations) or a stellar particle (in SPH simulations) respectively.

## Acknowledgments

We are very grateful to our CLUES colleagues (<http://clues-project.org>) for their productive and fruitful collaboration. Without them, this review would have been impossible. GY thanks the Spanish’s MINECO and MICINN for supporting his research through different projects: AYA2009-13875-C03-02, FPA2009-08958, AYA2012-31101, FPA2012-34694 and Consolider Ingenio SyeC CSD2007-0050. He also acknowledge support from the Comunidad de Madrid through the ASTROMADRID PRICIT project (S2009/ESP-1496). YH acknowledges the support of the Israel Science Foundation (ISF 1013/13). SG and YH have been partially supported by the Deutsche Forschungsgemeinschaft under the grant GO563/21 – 1. We also thank the Spanish MULTIDARK Consolider project (CSD2009-0006) and the Schonbrunn Fellowship at the Hebrew University Jerusalem for supporting our collaboration.

The simulations described here have been performed on different supercomputers at the Leibniz Rechenzentrum Munich (LRZ), the Barcelona Supercomputer Center (BSC) and the Juelich Supercomputing Center (JSC).

## References

- Aragón-Calvo, M.A., Jones, B.J.T., van de Weygaert, R., van der Hulst, J.M., 2007. The multiscale morphology filter: identifying and extracting spatial patterns in the galaxy distribution. *A&A* 474, 315–338. doi:10.1051/0004-6361:20077880, arXiv:0705.2072.
- Asaka, T., Shaposhnikov, M., 2005. The  $\mu\nu$ MSM, dark matter and baryon asymmetry of the universe [rapid communication]. *Physics Letters B* 620, 17–26. doi:10.1016/j.physletb.2005.06.020, arXiv:arXiv:hep-ph/0505013.
- Babcock, H.W., 1939. The rotation of the Andromeda Nebula. *Lick Observatory Bulletin* 19, 41–51.
- Behroozi, P.S., Marchesini, D., Wechsler, R.H., Muzzin, A., Papovich, C., Stefanon, M., 2013. Using Cumulative Number Densities to Compare Galaxies across Cosmic Time. *ApJLett* 777, L10. doi:10.1088/2041-8205/777/1/L10, arXiv:1308.3232.
- Benítez-Llambay, A., Navarro, J.F., Abadi, M.G., Gottlöber, S., Yepes, G., Hoffman, Y., Steinmetz, M., 2013. Dwarf Galaxies and the Cosmic Web. *ApJLett* 763, L41. doi:10.1088/2041-8205/763/2/L41, arXiv:1211.0536.
- Bond, J.R., Kofman, L., Pogosyan, D., 1996. How filaments of galaxies are woven into the cosmic web. *Nature* 380, 603–+. doi:10.1038/380603a0, arXiv:arXiv:astro-ph/9512141.
- Bosma, A., 1978. The distribution and kinematics of neutral hydrogen in spiral galaxies of various morphological types. Ph.D. thesis. PhD Thesis, Groningen Univ., (1978).
- Boylan-Kolchin, M., Bullock, J.S., Kaplinghat, M., 2011. Too big to fail? The puzzling darkness of massive Milky Way subhaloes. *MNRAS* 415, L40–L44. doi:10.1111/j.1745-3933.2011.01074.x, arXiv:1103.0007.
- Boylan-Kolchin, M., Bullock, J.S., Kaplinghat, M., 2012. The Milky Way’s bright satellites as an apparent failure of  $\Lambda$ CDM. *MNRAS* 422, 1203–1218. doi:10.1111/j.1365-2966.2012.20695.x, arXiv:1111.2048.
- Boylan-Kolchin, M., Bullock, J.S., Sohn, S.T., Besla, G., van der Marel, R.P., 2013. The Space Motion of Leo I: The Mass of the Milky Way’s Dark Matter Halo. *ApJ* 768, 140. doi:10.1088/0004-637X/768/2/140, arXiv:1210.6046.
- Catena, R., Ullio, P., 2010. A novel determination of the local dark matter density. *JCAP* 8, 4. doi:10.1088/1475-7516/2010/08/004, arXiv:0907.0018.
- Courtois, H.M., Tully, R.B., 2012a. Cosmic Flows surveys and CLUES simulations. *Astronomische Nachrichten* 333, 436. doi:10.1002/asna.201211682, arXiv:1205.4627.
- Courtois, H.M., Tully, R.B., 2012b. Cosmicflows-2: Type Ia Supernova Calibration and  $H_0$ . *ApJ* 749, 174. doi:10.1088/0004-637X/749/2/174, arXiv:1202.3832.
- Cuesta, A.J., Jeltama, T.E., Zandanel, F., Profumo, S., Prada, F., Yepes, G., Klypin, A., Hoffman, Y., Gottlöber, S., Primack, J., Sánchez-Conde, M.A., Pfrommer, C., 2011. Dark Matter Decay and Annihilation in the Local Universe: Clues from Fermi. *ApJLett* 726, L6. doi:10.1088/2041-8205/726/1/L6, arXiv:1007.3469.
- de Blok, W.J.G., 2010. The Core-Cusp Problem. *Advances in Astronomy* 2010. doi:10.1155/2010/789293, arXiv:0910.3538.
- Di Cintio, A., Knebe, A., Libeskind, N.I., Brook, C., Yepes, G., Gottlöber, S., Hoffman, Y., 2013. Size matters: the non-universal density profile of subhaloes in SPH simulations and implications for the Milky Way’s dSphs. *MNRAS* 431, 1220–1229. doi:10.1093/mnras/stt240, arXiv:1204.0515.
- Di Cintio, A., Knebe, A., Libeskind, N.I., Hoffman, Y., Yepes, G., Gottlöber, S., 2012. Applying scale-free mass estimators to the Local Group in Constrained Local Universe Simulations. *MNRAS* 423, 1883–1895. doi:10.1111/j.1365-2966.2012.21013.x, arXiv:1204.0005.
- Diemand, J., Kuhlen, M., Madau, P., 2007. Dark Matter Substructure and Gamma-Ray Annihilation in the Milky Way Halo. *ApJ* 657, 262–270. doi:10.1086/510736, arXiv:arXiv:astro-ph/0611370.
- Doumler, T., Courtois, H., Gottlöber, S., Hoffman, Y., 2013a. Reconstructing cosmological initial conditions from galaxy peculiar velocities - II. The effect of observational errors. *MNRAS* 430, 902–911. doi:10.1093/mnras/sts603, arXiv:1212.2808.
- Doumler, T., Gottlöber, S., Hoffman, Y., Courtois, H., 2013b. Reconstructing cosmological initial conditions from galaxy peculiar velocities - III. Constrained simulations. *MNRAS* 430, 912–923. doi:10.1093/mnras/sts614, arXiv:1212.2810.
- Doumler, T., Hoffman, Y., Courtois, H., Gottlöber, S., 2013c. Reconstructing cosmological initial conditions from galaxy peculiar velocities - I. Reverse Zeldovich Approximation. *MNRAS* 430, 888–901. doi:10.1093/mnras/sts613, arXiv:1212.2806.
- Einasto, J., 2009. Dark Matter. *ArXiv e-prints* arXiv:0901.0632.
- Forero-Romero, J.E., Hoffman, Y., Bustamante, S., Gottlöber, S., Yepes, G., 2013. The Kinematics of the Local Group in a Cosmological Context. *ApJLett* 767, L5. doi:10.1088/2041-8205/767/1/L5, arXiv:1303.2690.
- Forero-Romero, J.E., Hoffman, Y., Gottlöber, S., Klypin, A., Yepes, G., 2009. A dynamical classification of the cosmic web. *MNRAS* 396, 1815–1824. doi:10.1111/j.1365-2966.2009.14885.x, arXiv:0809.4135.
- Forero-Romero, J.E., Hoffman, Y., Yepes, G., Gottlöber, S., Piontek, R., Klypin, A., Steinmetz, M., 2011. The dark matter assembly of the Local Group in constrained cosmological simulations of a  $\Lambda$  cold dark matter universe. *MNRAS* 417, 1434–1443. doi:10.1111/j.1365-2966.2011.19358.x, arXiv:1107.0017.
- Frenk, C.S., White, S.D.M., 2012. Dark matter and cosmic structure. *Annalen der Physik* 524, 507–534. doi:10.1002/andp.201200212, arXiv:1210.0544.
- Giovanelli, R., Haynes, M.P., Kent, B.R., Perillat, P., Catinella, B., Hoffman, G.L., Momjian, E., Rosenberg, J.L., Saintonge, A., Spekkens, K., Stierwalt, S., Brosch, N., Masters, K.L., Springob, C.M., Karachentsev, I.D., Karachentseva, V.E., Koopmann, R.A., Muller, E., van Driel, W., van Zee, L., 2005. The Arecibo Legacy Fast ALFA Survey. II. Results of Precursor Observations. *AJ* 130, 2613–2624. doi:10.1086/497432, arXiv:arXiv:astro-ph/0508300.
- Gnedin, O.Y., Ceverino, D., Gnedin, N.Y., Klypin, A.A., Kravtsov, A.V., Levine, R., Nagai, D., Yepes, G., 2011. Halo Contraction Effect in Hydrodynamic Simulations of Galaxy Formation. *ArXiv e-prints* arXiv:1108.5736.
- Gómez-Vargas, G.A., Fornasa, M., Zandanel, F., Cuesta, A.J., Muñoz, C., Prada, F., Yepes, G., 2012. CLUES on Fermi-LAT prospects for the extragalactic detection of  $\mu\nu$ SSM gravitino dark matter. *JCAP* 2, 1. doi:10.1088/1475-7516/2012/02/001, arXiv:1110.3305.

- Gomez-Vargas, G.A., Sanchez-Conde, M.A., Huh, J.H., Peiro, M., Prada, F., Morselli, A., Klypin, A., Cerdeno, D.G., Mambrini, Y., Munoz, C., 2013. Constraints on WIMP Annihilation for Contracted Dark Matter in the Inner Galaxy with the Fermi-LAT. ArXiv e-prints [arXiv:1308.3515](https://arxiv.org/abs/1308.3515).
- Governato, F., Zolotov, A., Pontzen, A., Christensen, C., Oh, S.H., Brooks, A.M., Quinn, T., Shen, S., Wadsley, J., 2012. Cuspy no more: how outflows affect the central dark matter and baryon distribution in  $\Lambda$  cold dark matter galaxies. *MNRAS* 422, 1231–1240. doi:10.1111/j.1365-2966.2012.20696.x, [arXiv:1202.0554](https://arxiv.org/abs/1202.0554).
- Haardt, F., Madau, P., 1996. Radiative Transfer in a Clumpy Universe. II. The Ultraviolet Extragalactic Background. *ApJ* 461, 20. doi:10.1086/177035, [arXiv:astro-ph/9509093](https://arxiv.org/abs/astro-ph/9509093).
- Hahn, O., Porciani, C., Carollo, C.M., Dekel, A., 2007. Properties of dark matter haloes in clusters, filaments, sheets and voids. *MNRAS* 375, 489–499. doi:10.1111/j.1365-2966.2006.11318.x, [arXiv:astro-ph/0610280](https://arxiv.org/abs/astro-ph/0610280).
- Herpich, J., Stinson, G.S., Macciò, A.V., Brook, C., Wadsley, J., Couchman, H.M.P., Quinn, T., 2013. MaGICC-WDM: The effects of Warm Dark Matter in hydrodynamical simulations of disc galaxy formation. ArXiv e-prints [arXiv:1308.1088](https://arxiv.org/abs/1308.1088).
- Heß, S., Kitaura, F.S., Gottlöber, S., 2013. Simulating structure formation of the Local Universe. *MNRAS* 435, 2065–2076. doi:10.1093/mnras/stt1428, [arXiv:1304.6565](https://arxiv.org/abs/1304.6565).
- Hoffman, Y., Metuki, O., Yepes, G., Gottlöber, S., Forero-Romero, J.E., Libeskind, N.I., Knebe, A., 2012. A kinematic classification of the cosmic web. *MNRAS* 425, 2049–2057. doi:10.1111/j.1365-2966.2012.21553.x, [arXiv:1201.3367](https://arxiv.org/abs/1201.3367).
- Hoffman, Y., Ribak, E., 1991. Constrained realizations of Gaussian fields - A simple algorithm. *ApJLett* 380, L5–L8. doi:10.1086/186160.
- Hopkins, P.F., Bundy, K., Croton, D., Hernquist, L., Keres, D., Khochfar, S., Stewart, K., Wetzel, A., Younger, J.D., 2010. Mergers and Bulge Formation in  $\Lambda$ CDM: Which Mergers Matter? *ApJ* 715, 202–229. doi:10.1088/0004-637X/715/1/202, [arXiv:0906.5357](https://arxiv.org/abs/0906.5357).
- Jasche, J., Kitaura, F.S., Li, C., Enßlin, T.A., 2010. Bayesian non-linear large-scale structure inference of the Sloan Digital Sky Survey Data Release 7. *MNRAS* 409, 355–370. doi:10.1111/j.1365-2966.2010.17313.x, [arXiv:0911.2498](https://arxiv.org/abs/0911.2498).
- Kahn, F.D., Woltjer, L., 1959. Intergalactic Matter and the Galaxy. *ApJ* 130, 705. doi:10.1086/146762.
- Karachentsev, I.D., Karachentseva, V.E., Huchtmeier, W.K., Makarov, D.I., 2004. A Catalog of Neighboring Galaxies. *AJ* 127, 2031–2068. doi:10.1086/382905.
- Katz, N., Weinberg, D.H., Hernquist, L., 1996. Cosmological Simulations with TreeSPH. *ApJS* 105, 19. doi:10.1086/192305, [arXiv:astro-ph/9509107](https://arxiv.org/abs/astro-ph/9509107).
- Kitaura, F.S., Angulo, R.E., Hoffman, Y., Gottlöber, S., 2012. Estimating cosmic velocity fields from density fields and tidal tensors. *MNRAS* 425, 2422–2435. doi:10.1111/j.1365-2966.2012.21589.x, [arXiv:1111.6629](https://arxiv.org/abs/1111.6629).
- Klypin, A., Hoffman, Y., Kravtsov, A.V., Gottlöber, S., 2003. Constrained Simulations of the Real Universe: The Local Supercluster. *ApJ* 596, 19–33. doi:10.1086/377574, [arXiv:astro-ph/0107104](https://arxiv.org/abs/astro-ph/0107104).
- Klypin, A., Kravtsov, A.V., Bullock, J.S., Primack, J.R., 2001. Resolving the Structure of Cold Dark Matter Halos. *ApJ* 554, 903–915. doi:10.1086/321400, [arXiv:astro-ph/0006343](https://arxiv.org/abs/astro-ph/0006343).
- Klypin, A., Kravtsov, A.V., Valenzuela, O., Prada, F., 1999. Where Are the Missing Galactic Satellites? *ApJ* 522, 82–92. doi:10.1086/307643, [arXiv:astro-ph/9901240](https://arxiv.org/abs/astro-ph/9901240).
- Klypin, A.A., Trujillo-Gomez, S., Primack, J., 2011. Dark Matter Halos in the Standard Cosmological Model: Results from the Bolshoi Simulation. *ApJ* 740, 102. doi:10.1088/0004-637X/740/2/102, [arXiv:1002.3660](https://arxiv.org/abs/1002.3660).
- Knebe, A., Libeskind, N.I., Pearce, F., Behroozi, P., Casado, J., Dolag, K., Dominguez-Tenreiro, R., Elahi, P., Lux, H., Muldrew, S.I., Onions, J., 2013a. Galaxies going MAD: the Galaxy-Finder Comparison Project. *MNRAS* 428, 2039–2052. doi:10.1093/mnras/sts173, [arXiv:1210.2578](https://arxiv.org/abs/1210.2578).
- Knebe, A., Pearce, F.R., Lux, H., Ascasibar, Y., Behroozi, P., Casado, J., Moran, C.C., Diemand, J., Dolag, K., Dominguez-Tenreiro, R., Elahi, P., Falck, B., Gottlöber, S., Han, J., Klypin, A., Lukić, Z., Maciejewski, M., McBride, C.K., Merchán, M.E., Muldrew, S.I., Neyrinck, M., Onions, J., Planelles, S., Potter, D., Quilis, V., Rasera, Y., Ricker, P.M., Roy, F., Ruiz, A.N., Sgró, M.A., Springel, V., Stadel, J., Sutter, P.M., Tweed, D., Zemp, M., 2013b. Structure finding in cosmological simulations: the state of affairs. *MNRAS* 435, 1618–1658. doi:10.1093/mnras/stt1403, [arXiv:1304.0585](https://arxiv.org/abs/1304.0585).
- Kravtsov, A.V., Klypin, A., Hoffman, Y., 2002. Constrained Simulations of the Real Universe. II. Observational Signatures of Intergalactic Gas in the Local Supercluster Region. *ApJ* 571, 563–575. doi:10.1086/340046, [arXiv:astro-ph/0109077](https://arxiv.org/abs/astro-ph/0109077).
- Kroeger, T.L., Carlberg, R.G., 1991. The accuracy of galaxy masses from the timing argument. *ApJ* 376, 1–7. doi:10.1086/170249.
- Lemson, G., Kauffmann, G., 1999. Environmental influences on dark matter haloes and consequences for the galaxies within them. *MNRAS* 302, 111–117. doi:10.1046/j.1365-8711.1999.02090.x.
- Li, Y., Mo, H.J., Gao, L., 2008. On halo formation times and assembly bias. *MNRAS* 389, 1419–1426. doi:10.1111/j.1365-2966.2008.13667.x, [arXiv:0803.2250](https://arxiv.org/abs/0803.2250).
- Li, Y.S., White, S.D.M., 2008. Masses for the Local Group and the Milky Way. *MNRAS* 384, 1459–1468. doi:10.1111/j.1365-2966.2007.12748.x, [arXiv:0710.3740](https://arxiv.org/abs/0710.3740).
- Libeskind, N.I., Di Cintio, A., Knebe, A., Yepes, G., Gottloeber, S., Steinmetz, M., Hoffman, Y., Martinez-Vaquero, L.A., 2013a. Cold versus Warm Dark Matter simulations of a galaxy group. ArXiv e-prints [arXiv:1305.5557](https://arxiv.org/abs/1305.5557).
- Libeskind, N.I., Hoffman, Y., Forero-Romero, J., Gottlöber, S., Knebe, A., Steinmetz, M., Klypin, A., 2013b. The velocity shear tensor: tracer of halo alignment. *MNRAS* 428, 2489–2499. doi:10.1093/mnras/sts216, [arXiv:1210.4559](https://arxiv.org/abs/1210.4559).
- Libeskind, N.I., Hoffman, Y., Knebe, A., Steinmetz, M., Gottlöber, S., Metuki, O., Yepes, G., 2012. The cosmic web and the orientation of angular momenta. *MNRAS* 421, L137–L141. doi:10.1111/j.1745-3933.2012.01222.x, [arXiv:1201.3365](https://arxiv.org/abs/1201.3365).
- Lokas, E.L., 2009. The mass and velocity anisotropy of the Carina, Fornax, Sculptor and Sextans dwarf spheroidal galaxies. *MNRAS* 394, L102–L106. doi:10.1111/j.1745-3933.2009.00620.x, [arXiv:0901.0715](https://arxiv.org/abs/0901.0715).
- Lovell, M.R., Frenk, C.S., Eke, V.R., Jenkins, A., Gao, L., Theuns, T., 2013. The properties of warm dark matter haloes.

- ArXiv e-prints [arXiv:1308.1399](https://arxiv.org/abs/1308.1399).
- Lynden-Bell, D., 1981. The dynamical age of the local group of galaxies. *The Observatory* 101, 111–114.
- Massey, R., Rhodes, J., Ellis, R., Scoville, N., et al., 2007. Dark matter maps reveal cosmic scaffolding. *Nature* 445, 286–290. doi:10.1038/nature05497, [arXiv:astro-ph/0701594](https://arxiv.org/abs/astro-ph/0701594).
- Moore, B., Ghigna, S., Governato, F., Lake, G., Quinn, T., Stadel, J., Tozzi, P., 1999. Dark Matter Substructure within Galactic Halos. *ApJLett* 524, L19–L22. doi:10.1086/312287, [arXiv:astro-ph/9907411](https://arxiv.org/abs/astro-ph/9907411).
- Muñoz-Cuartas, J.C., Müller, V., Forero-Romero, J.E., 2011. Halo-based reconstruction of the cosmic mass density field. *MNRAS* 417, 1303–1317. doi:10.1111/j.1365-2966.2011.19344.x, [arXiv:1107.1062](https://arxiv.org/abs/1107.1062).
- Navarro, J.F., Frenk, C.S., White, S.D.M., 1997. A Universal Density Profile from Hierarchical Clustering. *ApJ* 490, 493. doi:10.1086/304888, [arXiv:astro-ph/9611107](https://arxiv.org/abs/astro-ph/9611107).
- Navarro, J.F., Ludlow, A., Springel, V., Wang, J., Vogelsberger, M., White, S.D.M., Jenkins, A., Frenk, C.S., Helmi, A., 2010. The diversity and similarity of simulated cold dark matter haloes. *MNRAS* 402, 21–34. doi:10.1111/j.1365-2966.2009.15878.x, [arXiv:0810.1522](https://arxiv.org/abs/0810.1522).
- Neistein, E., van den Bosch, F.C., Dekel, A., 2006. Natural downsizing in hierarchical galaxy formation. *MNRAS* 372, 933–948. doi:10.1111/j.1365-2966.2006.10918.x, [arXiv:astro-ph/0605045](https://arxiv.org/abs/astro-ph/0605045).
- Novikov, D., Colombi, S., Doré, O., 2006. Skeleton as a probe of the cosmic web: the two-dimensional case. *MNRAS* 366, 1201–1216. doi:10.1111/j.1365-2966.2005.09925.x, [arXiv:astro-ph/0307003](https://arxiv.org/abs/astro-ph/0307003).
- Oort, J.H., 1932. The force exerted by the stellar system in the direction perpendicular to the galactic plane and some related problems. *Bull. Astron. Inst. Netherlands* 6, 249.
- Papastergis, E., Martin, A.M., Giovanelli, R., Haynes, M.P., 2011. The Velocity Width Function of Galaxies from the 40% ALFALFA Survey: Shedding Light on the Cold Dark Matter Overabundance Problem. *ApJ* 739, 38. doi:10.1088/0004-637X/739/1/38, [arXiv:1106.0710](https://arxiv.org/abs/1106.0710).
- Partridge, C., Lahav, O., Hoffman, Y., 2013. Weighing the Local Group in the presence of dark energy. *MNRAS* 436, L45–L48. doi:10.1093/mnras/slt109, [arXiv:1308.0970](https://arxiv.org/abs/1308.0970).
- Piffi, T., Scannapieco, C., Binney, J., Steinmetz, M., Scholz, R.D., Williams, M.E.K., de Jong, R.S., Kordopatis, G., Matijevic, G., Bienayme, O., Bland-Hawthorn, J., Boeche, C., Freeman, K., Gibson, B., Gilmore, G., Grebel, E.K., Helmi, A., Munari, U., Navarro, J.F., Parker, Q., Reid, W.A., Seabroke, G., Watson, F., Wyse, R.F.G., Zwitter, T., 2013. The RAVE survey: the Galactic escape speed and the mass of the Milky Way. *ArXiv e-prints* [arXiv:1309.4293](https://arxiv.org/abs/1309.4293).
- Planck Collaboration, Ade, P.A.R., Aghanim, N., Armitage-Caplan, C., Arnaud, M., Ashdown, M., Atrio-Barandela, F., Aumont, J., Baccigalupi, C., Banday, A.J., et al., 2013. Planck 2013 results. XVI. Cosmological parameters. *ArXiv e-prints* [arXiv:1303.5076](https://arxiv.org/abs/1303.5076).
- Reiprich, T.H., Böhringer, H., 2002. The Mass Function of an X-Ray Flux-limited Sample of Galaxy Clusters. *ApJ* 567, 716–740. doi:10.1086/338753, [arXiv:astro-ph/0111285](https://arxiv.org/abs/astro-ph/0111285).
- Rocha, M., Peter, A.H.G., Bullock, J.S., Kaplinghat, M., Garrison-Kimmel, S., Oñorbe, J., Moustakas, L.A., 2013. Cosmological simulations with self-interacting dark matter - I. Constant-density cores and substructure. *MNRAS* 430, 81–104. doi:10.1093/mnras/sts514, [arXiv:1208.3025](https://arxiv.org/abs/1208.3025).
- Rubin, V.C., Ford, W.K.J., Thonnard, N., 1980. Rotational properties of 21 SC galaxies with a large range of luminosities and radii, from NGC 4605 ( $R = 4\text{ kpc}$ ) to UGC 2885 ( $R = 122\text{ kpc}$ ). *ApJ* 238, 471–487. doi:10.1086/158003.
- Sorce, J.G., Courtois, H.M., Gottloeber, S., Hoffman, Y., Tully, R.B., 2013. Simulations of the Local Universe Constrained by Observational Peculiar Velocities. *ArXiv e-prints* [arXiv:1311.2253](https://arxiv.org/abs/1311.2253).
- Sousbie, T., Pichon, C., Colombi, S., Novikov, D., Pogosyan, D., 2008. The 3D skeleton: tracing the filamentary structure of the Universe. *MNRAS* 383, 1655–1670. doi:10.1111/j.1365-2966.2007.12685.x, [arXiv:0707.3123](https://arxiv.org/abs/0707.3123).
- Springel, V., 2005. The cosmological simulation code GADGET-2. *MNRAS* 364, 1105–1134. doi:10.1111/j.1365-2966.2005.09655.x, [arXiv:astro-ph/0505010](https://arxiv.org/abs/astro-ph/0505010).
- Springel, V., Hernquist, L., 2002. Cosmological smoothed particle hydrodynamics simulations: the entropy equation. *MNRAS* 333, 649–664. doi:10.1046/j.1365-8711.2002.05445.x, [arXiv:astro-ph/0111016](https://arxiv.org/abs/astro-ph/0111016).
- Springel, V., Hernquist, L., 2003. Cosmological smoothed particle hydrodynamics simulations: a hybrid multiphase model for star formation. *MNRAS* 339, 289–311. doi:10.1046/j.1365-8711.2003.06206.x, [arXiv:astro-ph/0206393](https://arxiv.org/abs/astro-ph/0206393).
- Springel, V., Wang, J., Vogelsberger, M., Ludlow, A., Jenkins, A., Helmi, A., Navarro, J.F., Frenk, C.S., White, S.D.M., 2008. The Aquarius Project: the subhaloes of galactic haloes. *MNRAS* 391, 1685–1711. doi:10.1111/j.1365-2966.2008.14066.x, [arXiv:0809.0898](https://arxiv.org/abs/0809.0898).
- Strigari, L.E., 2013. Galactic searches for dark matter. *Physics Reports* 531, 1–88. doi:10.1016/j.physrep.2013.05.004, [arXiv:1211.7090](https://arxiv.org/abs/1211.7090).
- Tikhonov, A.V., Gottlöber, S., Yepes, G., Hoffman, Y., 2009. The sizes of minivoids in the local Universe: an argument in favour of a warm dark matter model? *MNRAS* 399, 1611–1621. doi:10.1111/j.1365-2966.2009.15381.x.
- Tikhonov, A.V., Klypin, A., 2009. The emptiness of voids: yet another overabundance problem for the  $\Lambda$  cold dark matter model. *MNRAS* 395, 1915–1924. doi:10.1111/j.1365-2966.2009.14686.x, [arXiv:0807.0924](https://arxiv.org/abs/0807.0924).
- Tollerud, E.J., Boylan-Kolchin, M., Barton, E.J., Bullock, J.S., Trinh, C.Q., 2011. Small-scale Structure in the Sloan Digital Sky Survey and  $\Lambda$ CDM: Isolated  $L^*$  Galaxies with Bright Satellites. *ApJ* 738, 102. doi:10.1088/0004-637X/738/1/102, [arXiv:1103.1875](https://arxiv.org/abs/1103.1875).
- Tonry, J.L., Dressler, A., Blakeslee, J.P., Ajhar, E.A., Fletcher, A.B., Luppino, G.A., Metzger, M.R., Moore, C.B., 2001. The SBF Survey of Galaxy Distances. IV. SBF Magnitudes, Colors, and Distances. *ApJ* 546, 681–693. doi:10.1086/318301, [arXiv:astro-ph/0011223](https://arxiv.org/abs/astro-ph/0011223).
- Tully, R.B., Courtois, H.M., 2012. Cosmicflows-2: I-band Luminosity-H I Linewidth Calibration. *ApJ* 749, 78. doi:10.1088/0004-637X/749/1/78, [arXiv:1202.3191](https://arxiv.org/abs/1202.3191).

- Tully, R.B., Courtois, H.M., Dolphin, A.E., Fisher, J.R., Héraudeau, P., Jacobs, B.A., Karachentsev, I.D., Makarov, D., Makarova, L., Mitronova, S., Rizzi, L., Shaya, E.J., Sorce, J.G., Wu, P.F., 2013. Cosmicflows-2: The Data. *AJ* 146, 86. doi:10.1088/0004-6256/146/4/86, arXiv:1307.7213.
- van de Hulst, H.C., Raimond, E., van Woerden, H., 1957. Rotation and density distribution of the Andromeda nebula derived from observations of the 21-cm line. *Bull. Astron. Inst. Netherlands* 14, 1.
- van der Marel, R.P., Besla, G., Cox, T.J., Sohn, S.T., Anderson, J., 2012. The M31 Velocity Vector. III. Future Milky Way M31-M33 Orbital Evolution, Merging, and Fate of the Sun. *ApJ* 753, 9. doi:10.1088/0004-637X/753/1/9, arXiv:1205.6865.
- Vera-Ciro, C.A., Helmi, A., Starkenburg, E., Breddels, M.A., 2013. Not too big, not too small: the dark haloes of the dwarf spheroidals in the Milky Way. *MNRAS* 428, 1696–1703. doi:10.1093/mnras/sts148, arXiv:1202.6061.
- Viel, M., Becker, G.D., Bolton, J.S., Haehnelt, M.G., 2013. Warm dark matter as a solution to the small scale crisis: New constraints from high redshift Lyman- $\alpha$  forest data. *Phys. Rev. D: Part. Fields* 88, 043502. doi:10.1103/PhysRevD.88.043502, arXiv:1306.2314.
- Vogelsberger, M., Zavala, J., Loeb, A., 2012. Subhaloes in self-interacting galactic dark matter haloes. *MNRAS* 423, 3740–3752. doi:10.1111/j.1365-2966.2012.21182.x, arXiv:1201.5892.
- Wang, H., Mo, H.J., Yang, X., van den Bosch, F.C., 2012. Reconstructing the cosmic velocity and tidal fields with galaxy groups selected from the Sloan Digital Sky Survey. *MNRAS* 420, 1809–1824. doi:10.1111/j.1365-2966.2011.20174.x, arXiv:1108.1008.
- Watkins, L.L., Evans, N.W., An, J.H., 2010. The masses of the Milky Way and Andromeda galaxies. *MNRAS* 406, 264–278. doi:10.1111/j.1365-2966.2010.16708.x, arXiv:1002.4565.
- Willick, J.A., Courteau, S., Faber, S.M., Burstein, D., Dekel, A., Strauss, M.A., 1997. Homogeneous Velocity-Distance Data for Peculiar Velocity Analysis. III. The Mark III Catalog of Galaxy Peculiar Velocities. *ApJS* 109, 333. doi:10.1086/312983, arXiv:arXiv:astro-ph/9610202.
- Wolf, J., Martinez, G.D., Bullock, J.S., Kaplinghat, M., Geha, M., Muñoz, R.R., Simon, J.D., Avedo, F.F., 2010. Accurate masses for dispersion-supported galaxies. *MNRAS* 406, 1220–1237. doi:10.1111/j.1365-2966.2010.16753.x, arXiv:0908.2995.
- Yepes, G., Kates, R., Khokhlov, A., Klypin, A., 1997. Hydrodynamical simulations of galaxy formation: effects of supernova feedback. *MNRAS* 284, 235–256. arXiv:arXiv:astro-ph/9605182.
- Zaroubi, S., Hoffman, Y., Dekel, A., 1999. Wiener Reconstruction of Large-Scale Structure from Peculiar Velocities. *ApJ* 520, 413–425. doi:10.1086/307473, arXiv:arXiv:astro-ph/9810279.
- Zavala, J., Jing, Y.P., Faltenbacher, A., Yepes, G., Hoffman, Y., Gottlöber, S., Catinella, B., 2009. The Velocity Function in the Local Environment from  $\Lambda$ CDM and  $\Lambda$ WDM Constrained Simulations. *ApJ* 700, 1779–1793. doi:10.1088/0004-637X/700/2/1779, arXiv:0906.0585.
- Zwicky, F., 1933. Die Rotverschiebung von extragalaktischen Nebeln. *Helvetica Physica Acta* 6, 110–127.